

1 Perturbing proteomes at single residue resolution using base  
2 editing

3

4

5 Philippe C Després<sup>1,2,3</sup>, Alexandre K Dubé<sup>1,2,3,4</sup>, Motoaki Seki<sup>5</sup>, Nozomu Yachie<sup>\*5,6,7</sup> and  
6 Christian R Landry<sup>\*1,2,3,4</sup>

7

8

9 1. Département de Biochimie, Microbiologie et Bio-informatique, Faculté de sciences et  
10 génie, Université Laval, Québec, Québec, G1V 0A6, Canada

11 2. PROTEO, le regroupement québécois de recherche sur la fonction, l'ingénierie et les  
12 applications des protéines, Université Laval, Québec, Québec, G1V 0A6, Canada

13 3. Centre de Recherche en Données Massives (CRDM), Université Laval, Québec,  
14 Québec, G1V 0A6, Canada

15 4. Département de Biologie, Faculté de sciences et Génie, Université Laval, Québec,  
16 Québec, G1V 0A6, Canada

17 5. Research Center for Advanced Science and Technology, Synthetic Biology Division,  
18 University of Tokyo, Tokyo, 4-6-1 Komaba, Meguro-ku, 153-8904, Japan

19 6. Department of Biological Sciences, Graduate School of Science, the University of  
20 Tokyo, Tokyo, Japan

21 7. Institute for Advanced Biosciences, Keio University, Tsuruoka, Japan

22 \*To whom correspondence should be addressed. CRL: Tel: 1-418-656-3954, Fax 1-  
23 418-656-7176, [christian.landry@bio.ulaval.ca](mailto:christian.landry@bio.ulaval.ca) NY: Tel +81-3-5452-5242 (x55242), Fax  
24 +81-3-5452-5241 (x55241), [yachie@synbiol.rcast.u-tokyo.ac.jp](mailto:yachie@synbiol.rcast.u-tokyo.ac.jp)

25 **Abstract**

26 Base editors derived from CRISPR-Cas9 systems and DNA editing enzymes offer an  
27 unprecedented opportunity for the precise modification of genes, but have yet to be used at a  
28 genome-scale throughput. Here, we test the ability of an editor based on a cytidine deaminase,  
29 the Target-AID base editor, to systematically modify genes genome-wide using the set of yeast  
30 essential genes. We tested the effect of mutating around 17,000 individual sites in parallel  
31 across more than 1,500 genes in a single experiment. We identified over 1,100 sites at which  
32 mutations have a significant impact on fitness. Using previously determined and preferred  
33 Target-AID mutational outcomes, we predicted the protein variants caused by each of these  
34 gRNAs. We found that gRNAs with significant effects on fitness are enriched in variants  
35 predicted to be deleterious by independent methods based on site conservation and predicted  
36 protein destabilization. Finally, we identify key features to design effective gRNAs in the context  
37 of base editing. Our results show that base editing is a powerful tool to identify key amino acid  
38 residues at the scale of proteomes.

## 39 Introduction

40 Recent technical advances have allowed the investigation of the genotype-phenotype map at  
41 high resolution by experimentally measuring the effect of all possible nucleotide substitutions in  
42 a short DNA sequence. While saturated mutagenesis informs us on the effect of many  
43 mutations, it usually covers a single locus or a fraction of it<sup>1,2</sup>. Because such data is only  
44 available at sufficient coverage for a very small number of proteins, general rules on substitution  
45 effects must be extrapolated to other, often unrelated proteins. At a lower level of resolution,  
46 genome-scale mutational data has mostly been acquired through large-scale loss-of-function  
47 strain collections, where the same genetic change (for example, complete gene deletion) is  
48 applied to all genes<sup>3-5</sup>. This approach is a powerful way to isolate each gene's contribution to a  
49 phenotype, including fitness, but limits our understanding of the role of specific positions within a  
50 locus.

51 CRISPR-Cas9 based approaches usually cause protein loss of function through indel formation<sup>6</sup>  
52 or by modifying gene expression levels<sup>7-9</sup> at many loci in parallel. Again, these approaches  
53 generally limit the information gain to one perturbation per locus. There is therefore a strong  
54 tradeoff between the resolution of the existing assays and the number of loci or genes  
55 investigated. Recent developments in the field now allow for the exploration of the effects of  
56 many mutations per gene across the genome. For instance, in yeast, methods for high  
57 throughput strain library construction have allowed the measurement of thousands of variant  
58 fitness effects in parallel across the genome<sup>10-14</sup>. These approaches rely on CRISPR-Cas9  
59 based genome modifications requiring the formation of double-strand breaks followed by repair  
60 using donor DNA, which often depends on complex strain and plasmid constructions. An  
61 alternative approach would be to use base editors, which allow the introduction of the mutations  
62 of interest directly in the genome by direct modification of DNA bases rather than DNA segment  
63 replacement.

64  
65 Base editors use DNA modifying enzymes fused to modified Cas9 or Cas12 proteins to create  
66 specific point mutations in a target genome<sup>15-17</sup>. Such base editors have recently been used to  
67 perform site-specific forward mutagenesis in human cell lines. The two main approaches,  
68 Targeted AID-mediated mutagenesis (TAM)<sup>18</sup> and CRISPR-X<sup>19</sup>, target specific regions of the  
69 genome where they induce mutations randomly. This generates a library of mutant genotypes  
70 that can be competed to find beneficial and deleterious variants under selective pressure. As  
71 the relative fitness measurements depend on targeted sequencing of the locus of interest, these  
72 approaches are difficult to adapt to high throughput multiplexed screens where tens of  
73 thousands of sites can be targeted within the same gRNA libraries.

74  
75 Here, we present a method that bridges the flexibility of Target-AID mutagenesis and the  
76 multiplexing capacities of genome editing depletion screens. By using a base editor with a  
77 narrow and well-defined activity window<sup>15</sup>, we selected gRNAs generating a limited number of  
78 predictable edits in yeast essential genes. This allowed us to use gRNAs as a readout for the  
79 effect of the mutations, similar to commonly used barcode-sequencing approaches to measure  
80 fitness effects.

## 81 **Results**

### 82 **Design of a base editing library targeting essential genes**

83 We used Target-AID mutagenesis to simultaneously assess mutational effects at over 17,000  
84 putative sites in the yeast genome. We scanned yeast essential genes for sites amenable to  
85 editing by the Target-AID base editor as well as targets with other specific properties, including  
86 intronic sequences. Because all essential genes have the same qualitative fitness effects when  
87 deleted<sup>20</sup>, focusing on these genes allowed us to limit the variation in fitness that could be due  
88 to the relative importance of individual genes for growth rather than to the importance of specific

89 positions within a locus. We excluded gRNAs that did not target between the 0.5th and 75th  
90 percentile of the length of annotated genes to limit position biases that could influence the effi-  
91 ciency of stop-codon generating guides<sup>21,22</sup>.

92  
93 To associate each gRNA in the library to specific base editing outcomes, we developed a simple  
94 model based on the yeast data included in the original Target-AID manuscript as well as our  
95 own work<sup>15,23</sup>. First, we expected that editing would mostly result in genotypes where only one  
96 nucleotide is edited in the activity window of the editor. Second, we predicted that the editing  
97 outcomes would mainly consist of C to G and C to T mutations and that the abundance of C to  
98 A products will be negligible. Finally, we expected that editing frequency ranks would follow the  
99 editing activity rankings already known from the initial characterization of Target-AID. Based on  
100 these criteria, we filtered out potential target sites where all three high editing rate positions (-  
101 19,-18 and -17) or those where both position -18 and -17 are cytosines and kept the remaining  
102 sites for inclusion in the gRNA library. The resulting library contained 40 000 gRNAs, of which  
103 ~35 000 targeted essential gene coding sequences and ~5000 other target types as shown in  
104 Supplementary Figure 1.

105  
106 Over 75% of target sequences in this set contained only one or two Cs in the extended activity  
107 window (positions -20 to -14), and as expected a general enrichment for cytosines in the high  
108 activity window (Supplementary Figure 2A-B). Because the goal of our experiment was to link  
109 specific mutations to fitness effects, co-editing of multiple nucleotides using an editor which  
110 does not channel mutations to a specific outcome has the potential to obscure the genotype re-  
111 sponsible for a fitness effect. To take this into account, we placed each gRNA in a co-editing  
112 risk category based on the presence and positions of cytosines in the activity window (See  
113 methods). Based on this metric, we found that over 80% of gRNAs fell either in the very low or

114 low risk category (Supplementary Figure 2C). If co-editing occurs, but the other mutated cyto-  
115 sine is part of the same codon as the intended target site, then any resulting fitness effects can  
116 still be linked to the perturbation of a specific amino acid. We found the proportion of gRNAs in  
117 the library for which this is true to be over 50%: when co-editing risk category is taken into ac-  
118 count, the proportion reaches ~90% (Supplementary Figure 2D). As Target-AID is known to per-  
119 form processive editing, a high co-editing risk might also be linked to higher overall editing  
120 rate<sup>15</sup>.

121

## 122 **Measurement of mutagenesis rate and outcomes of library gRNAs**

123 While the repair product outcomes of edits for gRNAs can be predicted with varying levels of  
124 accuracy for CRISPR-Cas9-based editing<sup>24</sup>, no such tools are available yet for base editing ap-  
125 plications. As such, the model we used to associate gRNAs in our library to mutational out-  
126 comes is only a parsimonious deduction based on the original Target-AID data and our previous  
127 work<sup>15,23</sup>. Furthermore, evaluating the activity of gRNAs for base editing remains difficult<sup>25</sup>. The  
128 measurement of fitness effects is not associated with a direct simultaneous measurement of  
129 mutagenesis rate in our experiment. As such, the absence of fitness effects for a gRNA can  
130 both be explained by either non-functional or low editing, or successful editing that resulted in  
131 mutations with no detectable fitness effects<sup>23</sup>. As our experiment focuses on the impact of tar-  
132 getted mutations on cell growth, the first group can be seen as false negatives, and the second  
133 as true negatives. While we can modulate the gRNA abundance variation threshold to minimize  
134 the risk of false positives, additional experimental data on mutagenesis success rates and edit-  
135 ing outcomes was required to assess which type of negative results would be dominant in our  
136 experiment.

137

138 To evaluate the performance of our model and the functionality of the library gRNAs, we per-  
139 formed a base editing time course experiment where mutagenesis rates and outcomes were  
140 measured by deep sequencing of the edited genomic loci (Supplementary Figure 3). To gain  
141 insights on the mutagenesis outcomes of different editing scenarios, we selected guides with  
142 different predicted patterns of cytosine presence in the Target-AID activity window (Figure 1A).  
143 We included 9 guides from the library isolated from the library quality control process (see  
144 methods), as well as three control gRNAs respectively targeting the pseudogene YCL074W, the  
145 non-essential gene *VPS17*, and *ADE1*, which can be used as a phenotypic marker. Most  
146 gRNAs could efficiently edit their respective targets, with 9 out of 12 gRNAs reaching mutation  
147 rates of 50% or higher (Figure 1B), consistent with previous results<sup>15,23</sup>. Replicates were highly  
148 correlated along different measurements with editing rates at the *CAN1* co-editing site being  
149 highly consistent (Supplementary Figure 4A-E). Only the gRNA targeting *SES1* was found to be  
150 inactive, and as such was excluded from downstream analysis. The very low editing rate ob-  
151 served for the gRNA targeting *SES1* is an example of unknown factors affecting mutagenesis  
152 efficiency that leads to false negatives in large-scale experiments.

153  
154 In our editing model, we first predict that single mutants would be the main mutagenesis out-  
155 come of the base editing process. We found this to be true for 9 gRNAs out of 10 with more  
156 than one cytosine in the Target-AID activity window (Figure 1C). Second, our model considers C  
157 to A editing to be rare and thus disregards them in favor of the more common C to G and C to T  
158 mutations. We observe this bias in the deep sequencing data (Figure 1D), with the median oc-  
159 cupancy of both C to G and C to T genotypes in edited alleles being much greater than C to A  
160 occupancy (C to T vs C to A:  $W=0$ ,  $p=1.73 \times 10^{-6}$ , C to G vs C to A:  $W=41$ ,  $p=8.19 \times 10^{-5}$ , two-sided  
161 wilcoxon signed rank test). Including these mutations as in our model leads to a median cover-  
162 age of 93% of mutagenesis outcomes. Our sequencing data also showed a greater prevalence  
163 of C to T mutations compared to C to G ( $W=112$ ,  $p=0.01$ ), but if absolute editing rate is taken

164 into account this difference disappears (Supplementary Figure 4F). Finally, in cases where mul-  
165 tiple editable nucleotides are present in the activity window of the base editor, our model uses  
166 the quantitative data of the original Target-AID manuscript to predict qualitatively which position  
167 should be edited at the highest frequency. We found that this prediction method of editing rank  
168 in the activity window matched with the experimental data in most cases (Figure 1E) which is  
169 unlikely to occur by chance ( $p \approx 0.0004$  based on  $1 \times 10^6$  random rank permutations). Globally, we  
170 found that the edited allele pool was mostly composed of the genotypes predicted by our model:  
171 for the 8 gRNAs with editing activity that came from the library, the median fraction of edited  
172 reads covered by our model was 69% (Figure 1F). In 7 out of 8 cases, the fractions of edited  
173 reads covered by the model was better than the 99th percentile of randomized outcome combi-  
174 nations and in 6 out of 8 cases and also superior to the 99.9th percentile. Overall, these results  
175 support that a large fraction of the gRNAs included in our library can edit their genomic targets  
176 in an efficient and predictable manner.

177

### 178 **High throughput screening using the gRNA library**

179 The gRNA library was cloned into a high-throughput co-selection base editing vector<sup>23</sup>. We  
180 performed pooled mutagenesis followed by bulk competition (Supplementary Figure 7) to  
181 identify mutations with significant fitness effects (Figure 2). As the relative abundance of each  
182 gRNA in the extracted plasmid pool depends on the abundance of the subpopulation of cells  
183 bearing these gRNAs, any fitness effect caused by the mutation they induce will influence their  
184 relative abundance. Variation in plasmid abundance was measured using targeted next-  
185 generation sequencing of the variable gRNA locus on the base editing vector in a manner  
186 similar to GeCKO approaches<sup>6,26</sup>.

187

188 After applying a stringent filtering threshold based on gRNA read count at the mutagenesis step  
189 (see methods), we identified a total of ~17,000 gRNAs for which we could evaluate fitness



190 effects. Replicate data for gRNAs passing the minimal read count selection criteria showed high  
191 correlation across experimental time points (Supplementary Figure 8) and cluster by  
192 experimental step (Supplementary Figure 9), showing that the approach is reproducible. Using  
193 the distribution of abundance variation of gRNAs between the start of the screen and the end of  
194 mock glucose induction as null distribution, we identified 1,118 gRNAs across 605 loci with  
195 significant negative effects (GNE) on cell survival or proliferation at a 5% False Discovery Rate  
196 (Figure 3A, Supplementary Figure 9 B and C). GNEs are distributed evenly across the yeast  
197 genome (Figure 3B), suggesting no inherent bias against specific regions. An example of gRNA  
198 abundance variation through time for all gRNAs (both GNEs and NSGs) targeting *GLN4* is  
199 shown in Figure 3C.

200  
201 Because our screen specifically targeted essential genes, many gRNAs cause mutations in  
202 highly conserved regions with high functional importance. To illustrate this, we focus on the  
203 highest scoring GNE targeting *GLN4*, a tRNA synthetase. The gRNA 33725 mutates a glycine  
204 at position 267 into either arginine or serine, and showed a dramatic drop in abundance in the  
205 large-scale experiment. To validate the deleteriousness of the predicted mutations, we  
206 transformed a centromeric plasmid bearing a wild-type or mutated copy of the gene under the  
207 control of its native promoter<sup>27</sup> in a heterozygous deletion background<sup>28</sup> (Supplementary figure  
208 10A). Glycine 267 is part of the “HIGH” motif, characteristic of class I tRNA synthetases, and is  
209 involved in ATP binding and catalysis and is highly conserved through evolution<sup>29</sup>. As expected,  
210 the region around the “HIGH” motif shows both a low evolutionary rate based on inter-species  
211 comparisons and a much lower variant density in yeast populations compared to other domains  
212 of Gln4 (Supplementary figure 10B), showing conservation both on a short and long timescales.  
213 Surprisingly, mutagenesis experiments in the bacterial homolog MetRS concluded that mutating  
214 this residue from glycine to alanine did not alter significantly catalysis while mutating it to proline

215 had a strong disruptive effect<sup>30</sup>. We found that mutating Gly 267 either to Arg or Ser was  
216 enough to cause protein loss of function (Figure 3D).

217 The five other sensitive sites identified in GLN4 by our screen were also clustered in regions  
218 with slow evolutionary rates. We found that one other GNE targeting residue D291 induced a  
219 highly deleterious mutation coupled with a neutral mutation as outcomes (D291E vs D291D,  
220 Supplementary Figure 11). We did not observe any discernible growth defect for the other GNE  
221 outcomes and as well as for the outcomes of 4 NSG targeting nearby amino acids. The other  
222 GNEs tested had markedly more positive scores than the one targeting G267, which would be  
223 consequent with a higher false positive rate close to the significance threshold. However, the  
224 case of the D291E/D291D pair, where a strong fitness effect is partially obscured by a neutral  
225 mutation produced by the other mutagenesis outcomes supports that sites of interest can be  
226 detected even close to the significance threshold. As we only tested two outcomes per gRNA, it  
227 is also possible that some of the abundance drops we measured were the result of mutations  
228 outside of our model, which are sometimes predicted to be more deleterious than the most likely  
229 mutations.

230

### 231 **Comparison of GNE induced mutations with variant effect predictions**

232 If GNEs indeed induce specific deleterious mutations, these mutations should be predicted to be  
233 more deleterious than those of Non-Significant gRNAs (NSG). We tested this using two recently  
234 published resources for variant effect prediction: Envision<sup>2</sup> and Mutfunc<sup>31</sup>. Envision is based on  
235 a machine learning approach that leverages large-scale saturated mutagenesis data of multiple  
236 proteins to perform quantitative predictions of missense mutation effects on protein function.  
237 The lower the Envision score, the higher the effect on protein function. Mutfunc aggregates  
238 multiple types of information such as residue conservation through the use of SIFT<sup>32</sup> as well as  
239 structural constraints to provide a binary prediction of variant effect based on multiple

240 quantitative and qualitative values. Mutations with a low SIFT score have a lower chance of  
241 being tolerated, while those with a positive  $\Delta\Delta G$  are predicted to destabilize protein structure or  
242 interactions. Both Envision and the Mutfunc aggregated SIFT data cover the majority of the  
243 most probable mutations generated by the gRNA library (Supplementary Figure 12A). The  
244 structural modeling information had much lower coverage, covering at best around 12% of the  
245 most probable mutations (Supplementary Figure 12B). As expected, mutations generated by  
246 GNEs showed significantly lower SIFT scores and showed enrichment for strong effects  
247 predicted by SIFT and Envision (Figure 4). Indeed, all four most probable substitutions created  
248 by GNEs are about twice more likely to be predicted to have a large deleterious effect by  
249 Envision or a very low chance of being tolerated as predicted by SIFT compared to NSG  
250 gRNAs. Envision scores across the proteome show a high level of homogeneity, with most  
251 mutations having a score between 0.94 and 0.96 (Supplementary Figure 12C). According to the  
252 original Envision manuscript, this should be predictive of a small decrease in protein function.  
253 As such, the shifts in score distributions between GNEs and NSGs are more subtle but still  
254 support that GNE induced mutations are generally more likely to be deleterious as well  
255 (Supplementary Figure 13A).

256  
257 Mutations with destabilizing effects as predicted by structural data also appeared to be enriched  
258 in GNEs predicted mutations but low residue coverage limits the strength of this association.  
259 This is supported by the raw  $\Delta\Delta G$  value distributions, which show a significant tendency for  
260 GNE mutations to be more destabilizing (Welch's t-test p-values for GNE vs NSG  $\Delta\Delta G$ : C-to-G  
261 #1 0.0001, C-to-T #1 0.0064, C-to-G #2 0.148, C-to-T #2 0.007, Supplementary Figure S13B-  
262 D). However, the shift in distribution only achieved significance for certain mutation predictions  
263 based on solved structures and homology models. While low residue coverage limits our  
264 statistical power, this weak apparent enrichment for mutations affecting protein stability may  
265 reflect the marginal stability of the target proteins<sup>33</sup>, resulting in individual destabilizing mutations

266 having a limited effects on fitness. As expected from known experimental data on mutagenesis  
267 outcomes<sup>15</sup>, signal was usually stronger for the most probable C to G mutation.

268

### 269 **Sensitive sites provide new biological insights**

270 Since Target-AID can only generate a limited range of amino acid substitutions from a specific  
271 coding sequence, we investigated whether any of these mutational patterns were enriched in  
272 GNEs (Figure 5A, source data in Supplementary tables 2, 3, and 4). We found deviations from  
273 random expectations in both C-to-G and C-to-T mutation ratios that drove the enrichment of  
274 several mutation combination. Three out of four of the mutation pair patterns involving glycine  
275 were enriched in GNEs. For example, the Glycine to Arginine or Serine substitutions (as  
276 exemplified by guide 33725 targeting *GLN4*) is the second most enriched pattern, being almost  
277 four-fold overrepresented in GNE outcomes. This pattern is consistent with the fact that Arginine  
278 has properties highly dissimilar to those of Glycine<sup>34</sup>, making these substitutions highly  
279 deleterious. Furthermore, as Glycine residues are often important components of cofactor  
280 binding motifs (eg.: Phosphates)<sup>35</sup> this observation might reflect a tendency for GNEs to alter  
281 these sites.

282

283 As expected, there is a strong enrichment within GNEs for patterns that result in mutation to  
284 stop codons: both C-to-G patterns (Y to stop: 3 fold enrichment,  $p=3.62 \times 10^{-11}$ , S to stop: 2.2 fold  
285 enrichment,  $p=0.0002$ ) but only one C-to-T pattern was overrepresented significantly (W to stop,  
286 4.6 fold enrichment,  $p=6.23 \times 10^{-15}$ ). Substitutions to stop codon in one outcome also drove  
287 enrichment in the other: for example, the link between Serine to Stop (C-to-G) appears to be the  
288 cause of the Serine to Leucine (C-to-T) overrepresentation. Both mutation pairs involving  
289 mutating a Tryptophan to a stop via a C-to-T mutation are enriched: this is not surprising, as the  
290 alternative mutations Tryptophan to Serine or Cysteine are also highly disruptive<sup>34</sup>. Changes  
291 between similar amino acids, which are expected to be tolerable, were also generally depleted

292 in GNE (ex.: the Alanine to Glycine/Valine pair). Mutations in intronic sequences and putative  
293 non-functional peptides were also underrepresented, as were most patterns leading to silent  
294 mutations (Figure 5A). These results show the power of this approach to discriminate important  
295 functional sites from more mutation tolerant ones across the genome.

296  
297 Interestingly, genes for which more than one GNE were detected were enriched for molecular  
298 function terms linked to cofactor binding (Supplementary Table 5). This suggests that the GNEs  
299 might indeed have a tendency to affect protein function through mechanisms other than protein  
300 or interaction interface destabilization. These protein properties depend on many residues,  
301 making them more robust to single amino acid substitutions, whereas cofactor binding may  
302 depend specifically on a handful of residues, making these sites critical for function. Using the  
303 Uniprot database<sup>37</sup>, we also examined whether gRNAs that target annotated binding sites or  
304 highly conserved motifs are more likely to affect fitness compared to other gRNAs targeting the  
305 same set of genes. We found a 3.5 fold enrichment for GNEs directly affecting these sites  
306 (49/188,  $\text{ratio}^{\text{GNE On}}=0.261$ , 447/5969  $\text{ratio}^{\text{GNE Off}}=0.0749$ , two-sided Fisher's exact test  
307  $p=3.54 \times 10^{-14}$ ) or residues in a two amino acid window around them (23/138,  $\text{ratio}^{\text{GNE near}}=0.167$ ,  
308 447/5969,  $\text{ratio}^{\text{GNE Off}}=0.0749$ , two-sided Fisher's exact test  $p=0.00048$ ).

309  
310 The precise targeting of our method also allows us to investigate amino acid residues with  
311 known functional annotations such as post-translational modifications. We found no significant  
312 enrichment for gRNAs mutating directly annotated PTMs ( $\text{ratio}^{\text{GNE PTM}} = 19/1118$ ,  $\text{ratio}^{\text{NSG PTM}}$   
313  $243/15536$ , Fisher's exact test  $p=0.71$ ). Most of these sites were phosphorylation sites (7),  
314 metal coordinating residues (5) and ubiquitination sites (4). This is consistent with the  
315 hypothesis that many PTM sites<sup>36</sup> may have little functional importance and thus mutations  
316 affecting them should not be significantly enriched for strong fitness effects compared to other  
317 possible mutations. The same was also observed for gRNAs mutating residues near known

318 PTMs that could disturb recognition sites (ratio<sup>GNE nearPTM</sup> = 130/1118, ratio<sup>NSG nearPTM</sup> =  
319 1698/15536, Fisher's exact test p=0.43). As we did not specifically target PTMs, our sample size  
320 is small and it should be noted that statistical power regarding these observations is limited.  
321  
322 However, GNEs that do target annotated PTM sites might provide additional evidence  
323 supporting the importance of these sites in particular. For example, the best scoring GNE in the  
324 well-studied transcriptional regulator *RAP1* is predicted to mutate residue T486. This threonine  
325 has been reported as phosphorylated in two previous studies<sup>38,39</sup>, but the functional importance  
326 of this phosphorylation has not been explored yet. Residue T486 is located in a disordered  
327 region in the DNA binding domains<sup>40</sup>, which part of the only *RAP1* fragment essential for cell  
328 growth<sup>41,42</sup>. Because the available wild-type *RAP1* plasmid (see methods) does not complement  
329 gene deletion growth phenotype, we used a different strategy for validation that relied on  
330 CRISPR-mediated knock-in (see methods and Supplementary Figure 14). We tested the effect  
331 of several predicted GNE induced mutations in *RAP1* targeting positions T486, A510, R523 and  
332 A540 (Figure 5B-C). We found that the predicted mutations at two of these positions, R523 and  
333 A540, were highly deleterious. While we could not validate that the two most likely mutations  
334 predicted to be caused by the GNE targeting T486 had a detectable fitness effect in these  
335 conditions, we found that phosphomimetic mutations at this position were lethal but most other  
336 amino acids were well tolerated. While we could validate that this gRNA indeed targeted a  
337 sensitive site, the outcomes predicted by our model did not have any detectable fitness effects.  
338 This showcases a limitation of our approach: the uncertainty in outcome prediction can  
339 complicate validation studies. As we only tested progeny survival on rich media and at a  
340 permissive temperature and the screen was performed in synthetic media at 30°C, these  
341 mutants might still affect cell phenotype but in an environment-dependent manner.  
342

343

#### 344 **gRNA properties influence mutagenesis efficiency**

345 There are still very few high-throughput experimental datasets available that allow the investiga-  
346 tion of which gRNA properties affect editing efficiency in the context of base editing. We there-  
347 fore sought to examine what gRNA and target sequence features could influence mutagenesis  
348 efficiency. To do so, we focused on the subset of gRNAs with the potential to generate stop  
349 codons (stop codon generating gRNAs, SGGs) in essential genes (Figure 6A). As gRNAs in our  
350 library were designed to target the first 75% of the coding sequences, successful stop codon  
351 generation in this subset of genes should often lead to a lethal loss of function<sup>13,22</sup>.

352

353 We found important variation in the ratio of GNE for the different types of SGGs (Figure 6B),  
354 with gRNAs targeting TGG (Trp) codons having the highest activity. This is in opposition to the  
355 general trend, as in general C to G mutation leading to stop codon formation had higher GNE  
356 ratios than the three other C-to-T alternatives. Overall, we observed significant GNE enrichment  
357 in SGGs which depend on the first C to G mutation to induce stop codon formation (Figure 6C).  
358 Multiple factors can explain the higher performance of TGG targeting gRNAs. First, as most of  
359 these sites have high co-editing risk scores because of the two consecutive cytosines, they  
360 might have increased editing rates due to processive co-editing events, increasing the chance  
361 of fitness effect detection. This phenomenon might also occur in non-SGG gRNAs (Supplemen-  
362 tary Figure 15A). Second, we found a significant enrichment in GNEs for gRNAs targeting the  
363 non-coding strand, even after excluding SGGs (Figure 6D). This effect might be explained by  
364 the higher repair efficiency in the transcribed strand in yeast<sup>43</sup>. Furthermore, as the non-coding  
365 strand is the one which is transcribed, a deamination event there might lead to consequences at  
366 the protein level more rapidly when the mutated coding sequence is transcribed. In contrast, the  
367 targeted chromosomal strand appears to be much less important (Supplementary Figure 15B).  
368 The variation in GNE ratio observed between the different SGG target codons might also reflect

369 *in vivo* DNA repair preferences that depend on sequence context, where different outcomes  
370 might be favored depending on the target sequence. For example, the CA di-nucleotide might  
371 favor C to G mutations, which would explain the low GNE ratio of CAA (Gln) targeting SGGs  
372 and the higher than average GNE ratio of TCA (Ser) targeting SGGs.

373  
374 Another parameter with a high impact on GNE enrichment in gRNA sets is the predicted melting  
375 temperature of the RNA-DNA duplex formed by the gRNA sequence and its target DNA se-  
376 quence (Supplementary Figure 15C-D). Both SGG and non-SGG gRNAs with low values have a  
377 lower chance of being detected as having effects, while gRNAs with higher values are enriched  
378 for GNEs (Figure 6E). This enrichment cannot be attributed to technical biases in library prepa-  
379 ration or high-throughput sequencing that would tend to lower their abundance as melting tem-  
380 perature shows practically no correlation with read count at any time point (Supplementary Fig-  
381 ure 16). Furthermore, this effect is not caused by target position bias within target genes or a  
382 strong correlation between GC content and the targeted position (Supplementary Figure 17).  
383 Even if binding energy is strongly correlated with GC content, there is still significant variation  
384 within gRNA sets with the same %GC (Figure 6F).

385

## 386 **Discussion**

387 Using targeted deep sequencing and high throughput screening, we investigated whether the  
388 Target-AID base editor is amenable for genome-scale targeted mutagenesis studies. We show  
389 that a prediction model based on known Target-AID properties can be used to predict the major  
390 mutational outcome of editing, even if multiple editable nucleotides are present in the activity  
391 window. Using yeast essential genes as a test case, we then applied this approach on a larger  
392 scale and identified hundreds of gRNAs targeting sensitive residues that have significant effects  
393 on cellular fitness when mutated. We could then verify orthogonally the effects of mutational  
394 outcomes of GNE using classical genetics approaches and show that they tend to overlap with



395 variants predicted to be deleterious. By focusing on a few highly relevant variant sets, we  
396 highlighted the power and potential of our approach to generate new biological insights. We  
397 then used this data to investigate which factors influence base editing efficiency and found  
398 multiple gRNAs and target properties that affect mutagenesis and that could be optimized for  
399 future experiments in specific genomic spaces.

400 In previously published methods such as TAM and CRISPR-X<sup>18,19</sup>, the semi-random nature of  
401 the editing forces the use of mutant allele frequencies as a readout for mutational fitness effects,  
402 potentially limiting the scale of the experiments because only one genomic region can be  
403 targeted at a time. To complement these approaches, we use more predictable base editing to  
404 increase dramatically the number of target loci, albeit at the cost of a lower mutational density.  
405 Our results demonstrate the feasibility of base editing screening at a large scale with  
406 applications beyond stop codon generation, and future developments will further enhance it. For  
407 instance, the use of a base editor with multiple possible mutagenesis outcomes complexifies the  
408 prediction of editing outcomes, which can, in turn, make GNE follow-up challenging. Using a  
409 base editor that channels mutational outcomes such as cytidine deaminase-uracil glycosylase  
410 inhibitor (UGI) fusion can address this problem<sup>15</sup> but decreases the number of mutations  
411 explored during the experiment. However, recently published data on cytidine deaminase-UGI  
412 fusion has shown they could lead to off-target editing in vivo at a much higher rate compared to  
413 adenine base editors or the Cas9 nuclease<sup>44,45</sup>. Although there is currently no high throughput  
414 data on the off-target activity of Target-AID, data generated in yeast in the original publication  
415 suggests far lower rates than those recently reported in mammalian cells<sup>15</sup>. Recently, Sadhu,  
416 Bloom et al examined the effects of premature stop codons (PTC) in essential genes using a  
417 high throughput variant construction method that relied on homology directed repair using a  
418 mutated repair template<sup>13</sup>. They observed that a significant fraction of PTCs can be tolerated,  
419 but only within the last 30 codons of a protein. Outside this window, they found no link between

420 PTC tolerance and position within the coding sequence, something which we also did not  
421 observe both for SGGs and non-SGG gRNAs (Supplementary Figure 17A-B).

422  
423 We provide key empirical data on gRNA dependant parameters that can be used to optimize  
424 base editing efficiency. Based on our results, selecting gRNAs with high binding energy to their  
425 genomic targets and favoring those which target the non-coding strand can increase the chance  
426 of high editing activity. Importantly, our observations differ from what has been reported for  
427 Cas9-based genome editing. High gRNA RNA/DNA duplex binding has instead been associated  
428 with lower mutagenesis efficiency<sup>46</sup>. Our data thus confirms the observation that parameters  
429 associated with Cas9 editing cannot readily be transferred to base editors<sup>47</sup>. Furthermore, the  
430 temperature at which experiments are performed might affect efficiency for certain gRNAs with  
431 low gRNA-DNA duplex binding energy and should be considered when designing base editing  
432 experiments in different organisms<sup>15</sup>. However, it remains to be confirmed whether the  
433 enrichment for certain gRNA properties we observed are specific to Target-AID or will also be  
434 transferable to other base editors as this may depend on the enzymatic properties of these  
435 proteins. Acquiring large paired gRNA and mutagenesis outcome datasets similar to those  
436 available for Cas9 genome editing<sup>24</sup> will allow for more refined models for rational base editing  
437 activity prediction.

438  
439 The field of base editing is rapidly evolving, with new tools being developed constantly. One of  
440 the most recent additions to this fast-growing toolkit are engineered Cas9 enzymes with  
441 broadened PAM specificities<sup>48</sup>, which have already been shown to be compatible with base  
442 editors. More flexible PAM requirements are especially useful for base editing applications, as  
443 they increase the number of sites to be edited and also the number of potential gRNAs per site,  
444 increasing the chances of choosing optimal properties and thus greater efficiency<sup>25</sup>. Our method

445 allows an experimental scale which bridges saturation mutagenesis methods and genome-wide  
446 knock-out studies, alleviating the current trade-off between mutational diversity and the number  
447 of targets genes to generate new biological insights.

448

## 449 **Methods**

### 450 **Generation of a gRNA library for Target-AID mutagenesis of essential genes in yeast**

451 The Target-AID base editor has an activity window between base 15 to 20 in the gRNA  
452 sequence starting from the PAM, and the efficiency at these different positions was  
453 characterized in Nishida *et al.* 2016. This allowed us to predict the mutational outcomes for a  
454 specific gRNA provided the number of editable bases in the window is not too high. To select  
455 gRNAs, we parsed a database of gRNA targets for the *S. cerevisiae* reference genome  
456 sequences (strain S288c)<sup>49</sup> and applied several selection criteria. Since the screen was to be  
457 performed in the BY4741 strain, all gRNAs (unique seed sequence, no NAG site) within the  
458 database were aligned to the reference genome of that strain using Bowtie<sup>50</sup>. Only gRNAs with  
459 a single perfect alignment were kept for subsequent steps. To select gRNAs amenable to  
460 Target-AID base editing, we selected gRNAs with cytosines within the highest activity window of  
461 the editor (positions -17 to -19 starting from the PAM). To limit the total number of possible  
462 mutational outcomes, gRNAs with three cytosines within the window were removed as well as  
463 those with two cytosines at the highest activity positions. Next, we filtered out any gRNA  
464 containing a BsaI restriction site to prevent errors during the library cloning step.

465 The list of essential genes (n=1156)<sup>3,4</sup> was used to discriminate between gRNAs targeting  
466 essential or non-essential genes (retrieved from [http://www-](http://www-sequence.stanford.edu/group/yeast_deletion_project/Essential_ORFs.txt)  
467 [sequence.stanford.edu/group/yeast\\_deletion\\_project/Essential\\_ORFs.txt](http://www-sequence.stanford.edu/group/yeast_deletion_project/Essential_ORFs.txt)). Among non-essential  
468 genes, data from Qian *et al.* 2012<sup>51</sup> was used to create categories of fitness effects. If the  
469 fitness score (averaged across media and replicates) of a gene was below 0.75, it was  
470 categorized as “high effect” on fitness. We excluded auxotrophic marker genes as well as  
471 *CAN1*, *LYP1*, and *FCY1* because those could be used as co-selection markers<sup>23</sup>. Gene  
472 deletions with an averaged fitness score between 0.999 and 1.001 were categorized as having  
473 “no detectable effect” on fitness. We selected gRNAs targeting essential and high effect genes,  
474 as well as gRNAs targeting a set of 38 randomly chosen no effect genes. To further limit the

475 space of gRNAs examined, only gRNAs mapping from the 0.5<sup>th</sup> percent to the 75<sup>th</sup> percent of  
476 coding sequences were chosen. We also added gRNAs targeting all known yeast introns (Ares  
477 lab Database 4.3)<sup>52</sup> and putative non-functional peptides<sup>53</sup> selected with the same strategy  
478 except for the constraints on gRNA position within the sequence of interest. This resulted in a  
479 set of 39,989 gRNAs: library properties are summarized in Supplementary Figure 1. To assign a  
480 co-editing risk score to each gRNA, we defined four categories using the extended activity  
481 window sequence composition shown in Table 1.

482  
483

**Table 1: Sequence patterns of co-editing risk categories**

Co-editing risk category	Very Low	Low	Moderate	High
Sequence patterns	NCDDDNN NDCDDNN NDDCDNN	NCDDCNN NDCDCNN NDDCCNN	NCDCNNN	NCCDNNN

484 N = any nucleotide, D = A or T or G

485

### 486 **Library construction**

487 The plasmids, oligonucleotides, and media used in this study are listed in as Supplementary  
488 tables 6, 7 and 8 respectively. The oligo pool was synthesized by Arbor Biosciences (Michigan,  
489 USA) and was cloned into the pDYSCO vector using Golden Gate Assembly (New England  
490 Biolabs, Massachusetts, USA) with the following reaction parameters:

NEB GG buffer 10X	2 $\mu$ l
pDYSCO [75ng/ $\mu$ l]	1 $\mu$ l
Oligo pool [2ng/ $\mu$ l]	1 $\mu$ l
NEB GG mix	1 $\mu$ l
Water	15 $\mu$ l

491

492 The ligation mix was transformed in *E. coli* strain MC1061 (*[araD139]<sub>B/r</sub>  $\Delta$ (araA-leu)7697*  
493  *$\Delta$ lacX74 galK16 galE15(GalS)  $\lambda$ - e14- mcrA0 relA1 rpsL150(strR) spoT1 mcrB1 hsdR2)*<sup>54</sup> using

494 a standard chemical transformation protocol and plated on ampicillin selective media to select  
495 for transformants. Serial dilution of cells after outgrowth were plated and then used to calculate  
496 the total number of clones produced by the cloning reaction. Quality control of the assembly was  
497 performed by Sanger sequencing ~10 clones per assembly reaction. Cells were scraped from  
498 plates by adding ~5 ml of sterile water, incubating a few minutes at room temperature, and then  
499 using a glass rake to resuspend colonies. Resuspended plates were then pooled together in a  
500 single flask per reaction, which was then used to make glycerol stocks of the library and cell  
501 pellets for plasmid extraction. The Qiagen Midi-Prep kit (Qiagen, Germany) was used to extract  
502 plasmid DNA from cell pellets by following the manufacturer's instructions. The DNA  
503 concentration of each eluate was then measured using a NanoDrop (ThermoFisher,  
504 Massachusetts, USA), and a normalized master library for yeast transformation was assembled  
505 by combining equal quantities of each assembly pool.

#### 506 **Base editing time course and library preparation for deep sequencing**

507 Cells were co-transformed with pKN1252 and the pDYSCO plasmid bearing the gRNA of  
508 interest using the protocol described below for the large-scale experiment. Transformant plates  
509 were scraped by adding ~5 ml of sterile water, incubating a few minutes at room temperature,  
510 and then using a glass rake to resuspend colonies. The resuspended cells (one pool per guide)  
511 were used to inoculate two replicate cultures per guide. Cells went through the same induction  
512 protocol as for the large-scale experiment, but scaled down to a 24 deepwell plate (see  
513 Supplementary Figures 3 and 7). The volumes used were: 3 ml for the initial SC-UL+glucose  
514 culture, 4 ml for the SC-UL+glycerol step, 3 ml for the SC-UL+galactose step, and 3 ml for the  
515 liquid canavanine co-selection step. At the end of the galactose induction step, 100  $\mu$ l of a  
516 1/2000 dilution of each well was plated on SC-ULR+canavanine solid media to obtain editing  
517 survivor colonies. At the glycerol to galactose media switch, a ~1 OD pellet was sampled by  
518 spinning cells at 13 200 RPM and removing the media. Cell pellets were then stored at -80°C for

519 subsequent DNA extraction. The same method was used to sample ~1 OD at T=6 hours in  
520 galactose, ~2 OD at T=12 hours in galactose, and ~3 OD at the end of canavanine co-selection.  
521 Plates with selected colonies (edited at the *CAN1* locus) were soaked in water and scraped, and  
522 1.4 ml of the resulting cell suspension was sampled and stored.

523  
524 Genomic DNA was extracted from cell pellets using a standard phenol-chloroform method from  
525 each sample<sup>55</sup> and quantified by NanoDrop (Thermo fisher, Massachusetts, USA). For each  
526 sample, we aimed to sequence both the target edit site and the *CAN1* co-selection edit site. To  
527 multiplex the 240 samples in the same sequencing library, we used the row-column-plate-  
528 indexed PCR (RCP-PCR) approach<sup>56</sup>. Briefly, each target locus was amplified from genomic  
529 DNA and universal adapter sequences were added to each end of the amplicon. A 1/2500  
530 dilution of the resulting product was then used as template with a set of 10 (rows) by 12  
531 (column) primers used to index each sample in a second PCR reaction. All samples for the  
532 same locus were then pooled together and normalized according to electrophoresis gel band  
533 intensity and then purified using magnetic beads. A third and final PCR reaction on the purified  
534 pools was then used to add plate indexes and Illumina adapters: this reaction was performed in  
535 quadruplicate and the products from the four reactions were pooled together for purification.  
536 Sequencing was performed using the MiSeq Reagent Kit v3 on an Illumina MiSeq for 600 cycles  
537 (IBIS sequencing platform, Université Laval).

538  
539 After sequencing, samples were demultiplexed using a custom python script with the reads  
540 being subdivided in four (plate barcode forward, row barcode, column barcode and plate  
541 barcode reverse). After demultiplexing, the forward and reverse reads were merged using the  
542 PANDA-Seq software<sup>57</sup>. Reads were then aligned to reference locus sequences using the  
543 Needle software from EMBOSS<sup>58</sup>. A custom script was then used to parse the alignments and

544 extract genotype information for each read. The sequencing reads for the base editing deep  
545 sequencing experiment were deposited on the NCBI SRA as accession number PRJNA552472.  
546

#### 547 **Library transformation in yeast**

548 Competent BY4741 (*MATa his3Δ1 leu2Δ0 met15Δ0 ura3Δ0*) cells were first transformed with  
549 the pKN1252 (p315-GalL-Target-AID) plasmid using a standard lithium acetate method.  
550 Transformants were selected by plating cells on SC-L. After 48 h of growth, multiples colonies  
551 were used to inoculate a starter liquid culture for competent cells preparation using the standard  
552 lithium acetate protocol<sup>59</sup>: a culture volume of 200 ml was used to generate enough competent  
553 cells for mass transformation. The large-scale library transformation was performed by  
554 combining 40 transformation reactions performed with 40 ul of competent cells and 5 ul of  
555 plasmid library (240 ng/ul) after the outgrowth stage and plating 100 ul aliquots on SC-UL: cells  
556 were then allowed to grow at 30°C for 48 h. A 1/1000 serial dilution of the cell recovery was  
557 plated in 5 replicates and used to calculate the number of transformants obtained. The total  
558 number of transformants reached  $3.48 \times 10^6$  CFU, corresponding to about 100X coverage of the  
559 plasmid pool.

#### 560 **Target-AID mutagenesis and competition screening**

561 The mutagenesis protocol is an upscaled version of our previously published method<sup>23</sup> and is  
562 shown in Supplementary Figure 7. Transformants were scraped by spreading 5 ml sterile water  
563 on plates and then resuspending cells using a glass rake. All plates were pooled together in the  
564 same flask, and the OD of the yeast resuspension was measured using a Tecan Infinite F200  
565 plate reader (Tecan, Switzerland). Pellets corresponding to about  $6 \times 10^8$  cells were washed  
566 twice with SC-UL without a carbon source and then used to inoculate a 100 ml SC-UL +2%  
567 glucose culture at 0.6 OD two times to generate replicates A and B. Cells were allowed to grow  
568 for 8 hours before  $1 \times 10^9$  cells were pelleted and used to inoculate a 100 ml SC-UL + 5%



569 glycerol culture. After 24 hours,  $5 \times 10^8$  cells were pelleted and either put in SC-UL + 5%  
570 galactose for mutagenesis or SC-UL + 5% glucose for a mock induction control. Target-AID  
571 expression (from pKN1252) was induced for 12 hours before  $1 \times 10^8$  cells were pelleted and  
572 used to inoculate a canavanine (50  $\mu\text{g/ml}$ ) co-selection culture in SC-ULR. After 16 hours of  
573 incubation,  $5 \times 10^7$  cells of each culture were used to inoculate 100 ml SC-UR, which was grown  
574 for 12 hours before  $5 \times 10^7$  cells were used to inoculate a final 100 ml SC-UR culture which was  
575 grown for another 12 hours. Cell pellets were washed with sterile water between each step, and  
576 all incubation occurred at 30°C with agitation.  $\sim 2 \times 10^7$  cells were taken for plasmid DNA  
577 extraction at the end of each mutagenesis and competition screening step.

#### 578 **Yeast plasmid DNA extraction**

579 Yeast plasmid DNA was extracted using the ChargeSwitch Plasmid Yeast Mini Kit (Invitrogen,  
580 California, USA) by following the manufacturer's protocol with minor modifications: Zymolase  
581 4000 U/ml (Zymo Research, California, USA) was used instead of lyticase, and cells were  
582 incubated for 1 hour at room temperature, one min at -80°C, and then incubated for another 15  
583 minutes at room temperature before the lysis step. Plasmid DNA was eluted in 70  $\mu\text{l}$  of E5 buffer  
584 (10 mM Tris-HCl, pH 8.5) and stored at -20°C for use in library preparation.

#### 585 **Next-generation library sequencing preparation**

586 Libraries were prepared by using two PCR amplification steps, one to amplify the gRNA region  
587 of the pDSYCKO plasmid pool and the second to add sample barcodes as well as the Illumina  
588 p5 and p7 sequences<sup>60</sup>. Oligonucleotides for library preparation are shown in the first part of the  
589 oligonucleotide table. Reaction conditions for the first PCR were as follows:

590

Phusion HF buffer (NEB) 5X	5 $\mu$ l
dNTPs 10 mM	0.5 $\mu$ l
pDYSCO_gRNA_for 10 $\mu$ M	1.25 $\mu$ l
pDYSCO_gRNA_rev 10 $\mu$ M	1.25 $\mu$ l
Phusion polymerase	0.5 $\mu$ l
Template DNA (<1 ng/ $\mu$ l)	5 $\mu$ l
PCR grade water	11.7 $\mu$ l

591

592 Thermocycler protocol:

Temperature ( $^{\circ}$ C)	Time (s)	Cycles
98	30	1
98	10	16
58	15	
72	5	
72	5	1

593

594 The resulting product was verified on a 2% agarose gel colored with Midori Green Advance  
595 (Nippon Genetics, Japan) and then gel-extracted and purified using the FastGene Gel/PCR  
596 Extraction Kit (Nippon Genetics, Japan). The purified products were used as the template for  
597 the second PCR reaction, with the following conditions:

Phusion Mastermix-HF (NEB)	10 $\mu$ l
P5-barcode-X oligo 1.333 $\mu$ M	3.75 $\mu$ l
P7-barcode-Y oligo 1.333 $\mu$ M	3.75 $\mu$ l
Template DNA (~1 ng/ $\mu$ l)	2.5 $\mu$ l

598

599 Thermocycler protocol:

Temperature (°C)	Time (s)	Cycles
98	30	1
98	10	15
60	10	
72	60	
72	300	1

600

601 PCR products were verified on a 2% agarose gel colored with Midori Green Advance (Nippon  
602 Genetics, Japan) and then gel-extracted and purified using the FastGene Gel/PCR Extraction  
603 Kit (Nippon Genetics, Japan). Library quality control and quantification were performed using  
604 the KAPA Library Quantification Kit for Illumina platforms (Kapa Biosystems, Massachusetts,  
605 USA) following the manufacturer's instructions. Libraries were then run on a single lane on  
606 HiSeq 2500 (Illumina, California, USA) with paired-end 150 bp in fast mode.

#### 607 **Large-scale screen sequencing data analysis**

608 The custom Python scripts used to analyze the are available on github  
609 (<https://github.com/landrylaboratory>), and packages and software used are presented in  
610 Supplementary table 9. Raw sequencing files have been deposited on the NCBI SRA,  
611 accession number PRJNA552472. Briefly, reads were separated into three subsequences for  
612 alignment: the P5 barcode, the gRNA, and the P7 barcode. Each of these was aligned using  
613 Bowtie<sup>50</sup> to an artificial reference genome containing either the barcodes or gRNA sequences  
614 flanked by the common amplicon sequences. The gRNA sequences are aligned both with 0 or 1  
615 mismatch allowed, and misalignment position and type were stored. Information on barcode and  
616 gRNA alignment for each read was stored and combined to generate a barcode count per  
617 library table, a list of mismatches in alignments for each gRNA in each library, as well as  
618 mismatch types and counts for the same gRNA across all libraries.

619 gRNAs absent from more than half of the libraries (4446 out of 39,989) were removed from the  
620 analysis before gRNA abundance calculations.

### 621 **Detecting mutations with high fitness effects**

622 Barcode sequencing competition experiments use DNA barcodes to measure the relative  
623 abundance of many different subpopulations of cells grown in the same pool (Robinson *et al.*  
624 2014). Since each gRNA is linked to its possible mutagenesis outcomes, we can use relative  
625 gRNA abundance to detect mutations with significant fitness effects. To do so, the  $\log_2$  of the  
626 relative abundance of a barcode after mutagenesis is compared with its abundance at the end  
627 of the screen:

$$\Delta \log_2_{gRNA} = \log_2\left(\frac{N_{reads_{gRNA}t_1}}{N_{readst_1}}\right) - \log_2\left(\frac{N_{reads_{gRNA}t_0}}{N_{readst_0}}\right)$$

628 For each gRNA, the measured fitness effect is the product of the effect of the mutational  
629 outcomes on growth and of the mutation rate within the cell subpopulation bearing this particular  
630 gRNA. Relative counts will also vary stochastically because of variation in sequencing coverage  
631 depending on the time point and replicate. To reduce the impact of these effects, a minimal read  
632 count at the end of the galactose induction step was used to filter out low abundance gRNAs.  
633 We found a minimal read threshold of  $n=54$  provided a good tradeoff between the number of  
634 gRNAs eligible for analysis and inter-replicate correlation.

635 To obtain a reference distribution of abundance variation for gRNAs, we fit a normal distribution  
636 to the  $\Delta \log_2$  z-score distribution of gRNAs between the start of the experiment (The glucose  
637 timepoint in Supplementary Figure 9) and the end of the mock glucose induction time point  
638 ( $n=7875$  values). The mock induction recapitulates the galactose induction time point, but using  
639 glucose as a sole carbon source so that Target-AID is not expressed. Using this reference  
640 distribution, we calculated a z-score for each gRNA during the competition experiment

641 independently for both replicates. We then averaged z-scores between replicates. We set a  
642 significance threshold such as that all gRNAs at z-scores for which the estimated False  
643 Discovery Rate ~5% and the False positive Rate ~0.2% are considered GNEs (Supplementary  
644 Figure 9 B and C).

### 645 **Complementation assays**

646 Experiments were performed in heterozygous deletion mutants from the YKO project  
647 heterozygous deletion strain set (Dharmacon, Colorado, USA). For each gene, a single colony  
648 streaked from the glycerol stock was used to prepare competent cells using the previously  
649 described lithium acetate protocol<sup>59</sup>. To generate mutant alleles of the genes of interest, we  
650 performed site-directed mutagenesis on the appropriate MoBY collection plasmid<sup>27</sup>. These  
651 centromeric plasmids encode the yeast gene of interest under the control of their native  
652 promoters and terminators. Mutagenesis reactions were performed with the following reaction  
653 setup:

654

Kapa HiFi buffer (Kapa biosciences) 5X	5 $\mu$ l
dNTPs 10 $\mu$ M	0.75 $\mu$ l
mutation_for 10 $\mu$ M (see table 7)	0.75 $\mu$ l
mutation_rev 10 $\mu$ M (see table 7)	0.75 $\mu$ l
Kapa Hot-start polymerase	0.5 $\mu$ l
Template plasmid DNA (15ng/ $\mu$ l)	0.75 $\mu$ l
PCR grade water	16.5 $\mu$ l

655

656 Thermocycler protocol:

Temperature ( $^{\circ}$ C)	Time (s)	Cycles
95	300	1

98	20	
60	15	20
72	720	
72	1080	1

657  
658 After amplification, the mutagenesis product was digested with DpnI for 2 hours at 37°C and 5 ul  
659 was transformed in *E. coli* strain BW23474 (F<sup>-</sup>,  $\Delta(\text{argF-lac})169$ ,  $\Delta\text{uidA4}::\text{pir-116}$ , *recA1*,  
660 *rpoS396(Am)*, *endA9(del-ins)::FRT*, *rph-1*, *hsdR514*, *rob-1*, *creC510*)<sup>61</sup>. Transformants were  
661 plated on 2YT+Kan+Chlo and grown at 37°C overnight. Plasmid DNA was then isolated from  
662 clones and sent for Sanger sequencing (CHUL sequencing platform, Université Laval, Québec  
663 City, Canada) to confirm mutagenesis success.

664 Competent cells of target genes were transformed with the appropriate mutant plasmids as well  
665 a the original plasmid bearing the wild-type gene and the empty vector<sup>62</sup>, and transformants  
666 were selected by plating on SC-U (MSG). Multiple independent colonies per transformation  
667 were then put on sporulation media until sporulation could be confirmed by microscopy. For  
668 tetrad dissection, cells were resuspended in 100ul 20T zymolyase (200mg/ml dilution in water)  
669 and incubated for 20 minutes at room temperature. Cells were then centrifuged and  
670 resuspended in 50ul 1M sorbitol before being streaked on a level YPD plate. All dissections  
671 were performed using a Singer SporePlay microscope (Singer Instruments, UK). Plate pictures  
672 were taken after five days incubation at room temperature except for the RAP1 plasmid  
673 complementation test for which the picture was taken after three days. Pictures are shown in  
674 Supplementary Image File 1.

675

676 **Strain construction for confirmations in *RAP1***

677 Because the MoBY collection plasmid for RAP1 cannot fully complement the gene deletion  
678 (Supplementary image file 1), we instead performed confirmations by engineering mutations a  
679 diploid strain to create heterozygous mutants. *RAP1* was first tagged with a modified version of  
680 fragment DHFR F[1,2] (the first half) of the mDHFR enzyme<sup>63</sup>. The mDHFR[1,2]-FLAG cassette  
681 was amplified using gene-specific primers and previously described reaction parameters<sup>63</sup>. Cells  
682 were transformed with the cassette using the previously described transformation protocol and  
683 were plated on YPD+Nourseothricine (YPD+Nat in Media table). Positive clones were identified  
684 by colony PCR and successful fragment fusion was confirmed by Sanger sequencing (CHUL  
685 sequencing platform). We then mated the confirmed clones with strain Y8205 (*Mata*  
686 *can1::STE2pr-his5 lyp1::STE3prLEU2 Δura3 Δhis3 Δleu2*, Kindly gifted by Charlie Boone) by  
687 inoculating a 4ml YPD culture with overnight starter cultures of both strains and letting the  
688 culture grow overnight. Cells were then streaked on YPD+Nat and diploid cells were identified  
689 by colony PCR using mating type diagnosis primers<sup>64</sup>.

690 To create heterozygous deletion mutants of the target gene, we amplified a modified version of  
691 the *URA3* cassettes that could then be targeted with the CRISPR-Cas9 system to integrate our  
692 mutations of interest using homologous recombination at the target locus. The oligonucleotides  
693 we used differ from those commonly used in that they amplify the cassette without the two LoxP  
694 sites present at both ends. We found it necessary to remove those sites as one common  
695 mutational outcome after introducing a double-stranded break in the *URA3* cassette was inter-  
696 LoxP site recombination without the integration of donor DNA at the target locus. These  
697 modified cassettes recombine with DNA upstream the target gene on one end and the mDHFR  
698 F[1,2] fusion on the other, ensuring that the heterozygous deletion is always performed at the  
699 locus that is already tagged. Cassettes were transformed using the standard lithium acetate  
700 method, and cells were plated on SC-U (MSG) selective media. Heterozygous deletion mutants  
701 were then confirmed by colony PCR.

## 702 **CRISPR-Cas9 mediated Knock-in of targeted mutations**

703 Mutant alleles of target genes were amplified in two fragments using template DNA from the  
704 haploid tagged strain (See Supplementary figure 14). The two fragments bearing mutations  
705 were then fused together by a second PCR round to form the final donor DNA. This DNA was  
706 then co-transformed with a plasmid bearing Cas9 and a gRNA targeting the URA3 cassette for  
707 HDR mediated editing using a standard protocol<sup>65</sup>. Clones were then screened by PCR to verify  
708 donor DNA and mutation integration at the target locus. The targeted region of *RAP1* was then  
709 Sanger sequenced (CHUL sequencing platform, Université Laval, Québec City, Canada) to  
710 confirm the presence of the mutation of interest. Heterozygous mutants were sporulated on  
711 solid media until sporulation could be confirmed by microscopy using the same protocol  
712 previously described. The plates were then replica plated on YPD+Nat media, and the pictures  
713 were taken after five days at room temperature (Supplementary Image File 2).

## 714 **Evolutionary rate measurements and protein variant abundance**

715 Evolutionary rates were calculated using the Rate4site software<sup>66</sup> using multiple sequence  
716 alignments and phylogenies from PhylomeDB V4<sup>67</sup> as input and using the raw calculated rates  
717 as output. Variant data was compiled using data from the 1002 Yeast Genome Project  
718 (<http://1002genomes.u-strasbg.fr/files/allReferenceGenesWithSNPsAndIndelsInferred.tar.gz>).  
719 Strain-specific protein coding sequence were aligned to the S288c sequence using Fastx36<sup>68</sup>  
720 with the following parameters: `fastx36 -p -s -VT10 -T 6 -m 10 -n -3`  
721 `querymultifasta.fasta ref_orf.db 12\> fasta_out`. Alignments were then parsed  
722 with a custom Python script to identify variants. Variant abundance was measured as the  
723 number of strains in the dataset in which a specific variant was found. If the coding sequence  
724 contained ambiguous nucleotides (ex.: R or Y), separate coding sequences were generated for  
725 each possibility and each possible variant was considered as a separate occurrence.



## 726 **Analysis of the properties of stop codon generating gRNAs**

727 To analyse the sequence and target properties of gRNA inducing the creation of stop codons,  
728 data from multiple sources was compiled. For each target gene, length and chromosomal strand  
729 was obtained from the Saccharomyces Genome Database using the Yeastmine query  
730 interface<sup>69</sup>. Distance to centromere was obtained by calculating the minimal distance between  
731 the start of the gene and one extremity of the centromere coordinates. RNA:DNA duplex melting  
732 temperature of gRNA sequence with target genomic DNA was calculated using the  
733 MeltingTemp module from Biopython<sup>70</sup>, which uses values taken from Sugimoto et al<sup>71</sup>.  
734 Correlation between gRNA/DNA duplex melting temperatures was assessed using Spearman's  
735 rank correlation.

## 736 **Variant effect prediction resources analysis and GO enrichment**

737 All prediction data except the Envision scores were extracted from the aggregated data of the  
738 Mutfunc database<sup>31</sup>. Precomputed values were downloaded directly from the FTP server  
739 ([http://ftp.ebi.ac.uk/pub/databases/mutfunc/mutfunc\\_v1/yeast/](http://ftp.ebi.ac.uk/pub/databases/mutfunc/mutfunc_v1/yeast/)). This database includes  
740 precomputed SIFT scores for 5498 yeast proteins, as well as predicted variant ddG values  
741 based on protein structure (n=1057), homology models (n=1703) and protein-protein interaction  
742 interfaces (n=1109). Mutations with  $\Delta\Delta G > 1$  considered destabilizing.

743 Precomputed values from Envision<sup>2</sup> were downloaded directly from the database website  
744 ([https://envision.gs.washington.edu/shiny/envision\\_new/](https://envision.gs.washington.edu/shiny/envision_new/), file yeast\_predicted\_2017-03-12.csv).  
745 This file contained 34857830 mutation effect predictions spread across 4011 genes. The  
746 distribution of Envision scores for the genes targeted in the experiment that are included in the  
747 database are shown in Supplementary Figure 12.

748 We downloaded the Uniprot database for yeast genes (query: uniprot-proteome\_UP000002311)  
749 with annotations covering the following properties: Metal binding, Nucleotide binding, Site, DNA

750 binding, Calcium binding, Binding site, Active site, Motif. We found that 6295 gRNAs targeted  
751 genes which have annotations in Uniprot, of which 519 were GNEs ( $\text{ratio}_{\text{all}}=0.0749$ ). Statistical  
752 enrichments were calculated using this set of gRNAs as the reference population. Gene  
753 enrichments were performed using the PANTHER gene list analysis tool<sup>72</sup>. The list of genes for  
754 which 2 or more GNEs were detected was tested for enrichment against all genes targeted by  
755 the library using Fisher's exact test and False Discovery Rate calculations. The Gene Ontology  
756 datasets used were: GO molecular function complete, GO biological process complete, and GO  
757 cellular component complete.

## 758 **Data Availability**

759 All raw sequencing data has been deposited on the NCBI as accession number PRJNA552472.  
760 The gRNA screen scores, predicted mutation outcomes, mutation effect predictors scores, as  
761 well as other relevant annotations are presented in Supplementary Dataset 1. Source image  
762 files for the tetrad dissections are presented as Supplementary Image 1 and 2.

## 763 **Code Availability**

764 The custom Python scripts used to analyze the are available on github  
765 (<https://github.com/landrylaboratory>), and packages and software used are presented in  
766 Supplementary table 9.

## 767 **Acknowledgments**

768 This work was supported by the Canadian Institutes of Health Research Foundation grant  
769 387697 to C.R.L., as well as project grants 364920, 384483, a Frederick Banting and Charles  
770 Best graduate scholarship and a Vanier graduate scholarship to P.C.D., by Université Laval via  
771 an André Darveau Fellowship to P.C.D., the Fonds Québécois de Recherche en Santé via a  
772 Master's training award to P.C.D. and the Japan Society for the Promotion of Science grant  
773 numbers S15734 and S17161 to C.R.L. and N.Y. The authors thank Mathieu Hénault, Johan

774 Hallin, and Dan Yamamoto Evans for comments on the manuscript, as well as Maria Isabel  
775 Acosta Lopez for assistance during the strain construction process.

## 776 **Author contributions**

777 PCD, AKD, NY and CRL designed research. PCD and AKD performed experiments. PCD and  
778 MS generated NGS sequencing data. All data analysis was performed by PCD with input from  
779 CRL. PCD and CRL wrote the manuscript with input from all authors.

## 780 **Conflict of interest**

781 None to declare

782

## 783 **References**

- 784 1. Fowler, D. M. & Fields, S. Deep mutational scanning: a new style of protein science. *Nat.*  
785 *Methods* **11**, 801–7 (2014).
- 786 2. Gray, V. E., Hause, R. J., Luebeck, J., Shendure, J. & Fowler, D. M. Quantitative  
787 Missense Variant Effect Prediction Using Large-Scale Mutagenesis Data. *Cell Syst.*  
788 (2018). doi:10.1016/j.cels.2017.11.003
- 789 3. Winzeler, E. A. *et al.* Functional characterization of the *S. cerevisiae* genome by gene  
790 deletion and parallel analysis. *Science (80-. )*. **285**, 901–906 (1999).
- 791 4. Giaever, G. *et al.* Functional profiling of the *Saccharomyces cerevisiae* genome. *Nature*  
792 **418**, 387–391 (2002).
- 793 5. *C. elegans* Deletion Mutant Consortium, T. C. *elegans* D. M. Large-Scale Screening for  
794 Targeted Knockouts in the *Caenorhabditis elegans* Genome. *G3*;  
795 *Genes/Genomes/Genetics* **2**, 1415–1425 (2012).
- 796 6. Shalem, O. *et al.* Genome-scale CRISPR-Cas9 knockout screening in human cells.  
797 *Science (80-. )*. **343**, 84–87 (2014).
- 798 7. Qi, L. S. *et al.* Repurposing CRISPR as an RNA-guided platform for sequence-specific  
799 control of gene expression. *Cell* **152**, 1173–83 (2013).
- 800 8. Sander, J. D. & Joung, J. K. CRISPR-Cas systems for editing, regulating and targeting  
801 genomes. *Nat. Biotechnol.* **32**, 347–55 (2014).
- 802 9. Smith, J. D. *et al.* Quantitative CRISPR interference screens in yeast identify chemical-  
803 genetic interactions and new rules for guide RNA design. *Genome Biol.* **17**, 45 (2016).

- 804 10. Sharon, E. *et al.* Functional Genetic Variants Revealed by Massively Parallel Precise  
805 Genome Editing. *Cell* (2018). doi:10.1016/j.cell.2018.08.057
- 806 11. Bao, Z. *et al.* Genome-scale engineering of *Saccharomyces cerevisiae* with single-  
807 nucleotide precision. *Nat. Biotechnol.* (2018). doi:10.1038/nbt.4132
- 808 12. Roy, K. R. *et al.* Multiplexed precision genome editing with trackable genomic barcodes in  
809 yeast. *Nat. Biotechnol.* (2018). doi:10.1038/nbt.4137
- 810 13. Sadhu, M. J. *et al.* Highly parallel genome variant engineering with CRISPR-Cas9. *Nat.*  
811 *Genet.* (2018). doi:10.1038/s41588-018-0087-y
- 812 14. Guo, X. *et al.* High-throughput creation and functional profiling of DNA sequence variant  
813 libraries using CRISPR-Cas9 in yeast. *Nat. Biotechnol.* (2018). doi:10.1038/nbt.4147
- 814 15. Nishida, K. *et al.* Targeted nucleotide editing using hybrid prokaryotic and vertebrate  
815 adaptive immune systems. *Science* (80-. ). **353**, 553–563 (2016).
- 816 16. Gaudelli, N. M. *et al.* Programmable base editing of A•T to G•C in genomic DNA without  
817 DNA cleavage. *Nature* **551**, 464–471 (2017).
- 818 17. Rees, H. A. & Liu, D. R. Base editing: precision chemistry on the genome and  
819 transcriptome of living cells. *Nat. Rev. Genet.* **19**, 770–788 (2018).
- 820 18. Ma, Y. *et al.* Targeted AID-mediated mutagenesis (TAM) enables efficient genomic  
821 diversification in mammalian cells. *Nat. Methods* **13**, 1029–1035 (2016).
- 822 19. Hess, G. T. *et al.* Directed evolution using dCas9-targeted somatic hypermutation in  
823 mammalian cells. *Nat. Methods* (2016). doi:10.1038/nmeth.4038
- 824 20. Giaever, G. *et al.* Functional profiling of the *Saccharomyces cerevisiae* genome. *Nature*  
825 **418**, 387–391 (2002).
- 826 21. Doench, J. G. *et al.* Rational design of highly active sgRNAs for CRISPR-Cas9-mediated  
827 gene inactivation. *Nat. Biotechnol.* **32**, 1262–1267 (2014).
- 828 22. Michel, A. H. *et al.* Functional mapping of yeast genomes by saturated transposition. *Elife*  
829 **6**, (2017).
- 830 23. Després, P. C., Dubé, A. K., Nielly-Thibault, L., Yachie, N. & Landry, C. R. Double  
831 Selection Enhances the Efficiency of Target-AID and Cas9-Based Genome Editing in  
832 Yeast. *G3 (Bethesda)*. g3.200461.2018 (2018). doi:10.1534/g3.118.200461
- 833 24. Allen, F. *et al.* Predicting the mutations generated by repair of Cas9-induced double-  
834 strand breaks. *Nat. Biotechnol.* (2019). doi:10.1038/nbt.4317
- 835 25. Dandage, R., Després, P. C., Yachie, N. & Landry, C. R. beditor: A Computational  
836 Workflow for Designing Libraries of Guide RNAs for CRISPR-Mediated Base Editing.  
837 *Genetics* **212**, 377–385 (2019).
- 838 26. Sanjana, N. E., Shalem, O. & Zhang, F. Improved vectors and genome-wide libraries for  
839 CRISPR screening. *Nat. Methods* **11**, 783–784 (2014).
- 840 27. Ho, C. H. *et al.* A molecular barcoded yeast ORF library enables mode-of-action analysis  
841 of bioactive compounds. *Nat. Biotechnol.* **27**, 369–377 (2009).
- 842 28. Giaever, G. *et al.* Genomic profiling of drug sensitivities via induced haploinsufficiency.

- 843 *Nat. Genet.* **21**, 278–83 (1999).
- 844 29. Eriani, G., Delarue, M., Poch, O., Gangloff, J. & Moras, D. Partition of tRNA synthetases  
845 into two classes based on mutually exclusive sets of sequence motifs. *Nature* **347**, 203–  
846 206 (1990).
- 847 30. Schmitt, E., Panvert, M., Blanquet, S. & Mechulam, Y. Transition state stabilization by the  
848 'high' motif of class I aminoacyl-tRNA synthetases: The case of *Escherichia coli*  
849 methionyl-tRNA synthetase. *Nucleic Acids Res.* (1995). doi:10.1093/nar/23.23.4793
- 850 31. Wagih, O. *et al.* A resource of variant effect predictions of single nucleotide variants in  
851 model organisms. *Mol. Syst. Biol.* **14**, e8430 (2018).
- 852 32. Ng, P. C. & Henikoff, S. SIFT: Predicting amino acid changes that affect protein function.  
853 *Nucleic Acids Res.* (2003).
- 854 33. DePristo, M. A., Weinreich, D. M. & Hartl, D. L. Missense meanderings in sequence  
855 space: a biophysical view of protein evolution. *Nat. Rev. Genet.* **6**, 678–687 (2005).
- 856 34. Sneath, P. H. Relations between chemical structure and biological activity in peptides. *J.*  
857 *Theor. Biol.* **12**, 157–95 (1966).
- 858 35. Copley, R. R. & Barton, G. J. A Structural Analysis of Phosphate and Sulphate Binding  
859 Sites in Proteins. *J. Mol. Biol.* **242**, 321–329 (1994).
- 860 36. Landry, C. R., Levy, E. D. & Michnick, S. W. Weak functional constraints on  
861 phosphoproteomes. *Trends Genet.* **25**, 193–7 (2009).
- 862 37. Bateman, A. UniProt: A worldwide hub of protein knowledge. *Nucleic Acids Res.* (2019).  
863 doi:10.1093/nar/gky1049
- 864 38. Albuquerque, C. P. *et al.* A multidimensional chromatography technology for in-depth  
865 phosphoproteome analysis. *Mol. Cell. Proteomics* **7**, 1389–96 (2008).
- 866 39. Holt, L. J. *et al.* Global analysis of Cdk1 substrate phosphorylation sites provides insights  
867 into evolution. *Science* **325**, 1682–6 (2009).
- 868 40. König, P., Giraldo, R., Chapman, L. & Rhodes, D. The crystal structure of the DNA-  
869 binding domain of yeast RAP1 in complex with telomeric DNA. *Cell* **85**, 125–36 (1996).
- 870 41. Graham, I. R., Haw, R. A., Spink, K. G., Halden, K. A. & Chambers, A. In vivo analysis of  
871 functional regions within yeast Rap1p. *Mol. Cell. Biol.* **19**, 7481–90 (1999).
- 872 42. Wu, A. C. K. *et al.* Repression of Divergent Noncoding Transcription by a Sequence-  
873 Specific Transcription Factor. *Mol. Cell* **72**, 942-954.e7 (2018).
- 874 43. Reis, A. M. C. *et al.* Targeted detection of in vivo endogenous DNA base damage reveals  
875 preferential base excision repair in the transcribed strand. *Nucleic Acids Res.* **40**, 206–  
876 219 (2012).
- 877 44. Jin, S. *et al.* Cytosine, but not adenine, base editors induce genome-wide off-target  
878 mutations in rice. *Science* eaaw7166 (2019). doi:10.1126/science.aaw7166
- 879 45. Zuo, E. *et al.* Cytosine base editor generates substantial off-target single-nucleotide  
880 variants in mouse embryos. *Science* (80-. ). eaav9973 (2019).  
881 doi:10.1126/SCIENCE.AAV9973

- 882 46. Wong, N., Liu, W. & Wang, X. WU-CRISPR: characteristics of functional guide RNAs for  
883 the CRISPR/Cas9 system. *Genome Biol.* **16**, 218 (2015).
- 884 47. Kim, D. *et al.* Genome-wide target specificities of CRISPR RNA-guided programmable  
885 deaminases. *Nat. Biotechnol.* (2017). doi:10.1038/nbt.3852
- 886 48. Nishimasu, H. *et al.* Engineered CRISPR-Cas9 nuclease with expanded targeting space.  
887 *Science* eaas9129 (2018). doi:10.1126/science.aas9129
- 888 49. Dicarlo, J. E. *et al.* Genome engineering in *Saccharomyces cerevisiae* using CRISPR-  
889 Cas systems. *Nucleic Acids Res.* **41**, 4336–4343 (2013).
- 890 50. Langmead, B., Trapnell, C., Pop, M. & Salzberg, S. L. Ultrafast and memory-efficient  
891 alignment of short DNA sequences to the human genome. *Genome Biol.* **10**, R25 (2009).
- 892 51. Qian, W., Ma, D., Xiao, C., Wang, Z. & Zhang, J. The Genomic Landscape and  
893 Evolutionary Resolution of Antagonistic Pleiotropy in Yeast. *Cell Rep.* **2**, 1399–1410  
894 (2012).
- 895 52. Grate, L. & Ares, M. Searching yeast intron data at Ares lab web site. *Methods Enzymol.*  
896 (2002). doi:10.1016/S0076-6879(02)50975-7
- 897 53. Smith, J. E. *et al.* Translation of Small Open Reading Frames within Unannotated RNA  
898 Transcripts in *Saccharomyces cerevisiae*. *Cell Rep.* **7**, 1858–1866 (2014).
- 899 54. Casadaban, M. J. & Cohen, S. N. Analysis of gene control signals by DNA fusion and  
900 cloning in *Escherichia coli*. *J. Mol. Biol.* **138**, 179–207 (1980).
- 901 55. Amberg, D. C., Burke, D. J. & Strathern, J. N. *Methods in Yeast Genetics: A Cold Spring  
902 Harbor Laboratory Course Manual, 2005 Edition. A Cold Spring Harbor Laboratory  
903 Course Manual* (2005).
- 904 56. Yachie, N. *et al.* Pooled-matrix protein interaction screens using Barcode Fusion  
905 Genetics. *Mol. Syst. Biol.* (2016). doi:10.15252/msb.20156660
- 906 57. Masella, A. P., Bartram, A. K., Truszkowski, J. M., Brown, D. G. & Neufeld, J. D.  
907 PANDAsq: Paired-end assembler for illumina sequences. *BMC Bioinformatics* (2012).  
908 doi:10.1186/1471-2105-13-31
- 909 58. Rice, P., Longden, L. & Bleasby, A. EMBOSS: The European Molecular Biology Open  
910 Software Suite. *Trends in Genetics* (2000). doi:10.1016/S0168-9525(00)02024-2
- 911 59. Gietz, R. D. & Schiestl, R. H. High-efficiency yeast transformation using the LiAc/SS  
912 carrier DNA/PEG method. *Nat. Protoc.* **2**, 31–34 (2007).
- 913 60. Yachie, N. *et al.* Pooled-matrix protein interaction screens using Barcode Fusion  
914 Genetics. *Mol. Syst. Biol.* **12**, 863 (2016).
- 915 61. Haldimann, A. *et al.* Altered recognition mutants of the response regulator PhoB: a new  
916 genetic strategy for studying protein-protein interactions. *Proc. Natl. Acad. Sci. U. S. A.*  
917 **93**, 14361–6 (1996).
- 918 62. Zhao, L. *et al.* A genome-wide imaging-based screening to identify genes involved in  
919 synphilin-1 inclusion formation in *Saccharomyces cerevisiae*. *Sci. Rep.* **6**, 30134 (2016).
- 920 63. Tarassov, K. *et al.* An in vivo map of the yeast protein interactome. *Science* **320**, 1465–  
921 70 (2008).

- 922 64. Huxley, C., Green, E. D. & Dunham, I. Rapid assessment of *S. cerevisiae* mating type by  
923 PCR. *Trends Genet.* **6**, 236 (1990).
- 924 65. Ryan, O. W., Poddar, S. & Cate, J. H. D. Crispr–cas9 genome engineering in  
925 *Saccharomyces cerevisiae* cells. *Cold Spring Harb. Protoc.* **2016**, 525–533 (2016).
- 926 66. Mayrose, I., Graur, D., Ben-Tal, N. & Pupko, T. Comparison of site-specific rate-inference  
927 methods for protein sequences: Empirical Bayesian methods are superior. *Mol. Biol.*  
928 *Evol.* (2004). doi:10.1093/molbev/msh194
- 929 67. Huerta-Cepas, J., Capella-Gutiérrez, S., Prysycz, L. P., Marcet-Houben, M. & Gabaldón,  
930 T. PhylomeDB v4: Zooming into the plurality of evolutionary histories of a genome.  
931 *Nucleic Acids Res.* (2014). doi:10.1093/nar/gkt1177
- 932 68. Pearson, W. R., Wood, T., Zhang, Z. & Miller, W. Comparison of DNA Sequences with  
933 Protein Sequences. *Genomics* **46**, 24–36 (1997).
- 934 69. Cherry, J. M. *et al.* *Saccharomyces* Genome Database: The genomics resource of  
935 budding yeast. *Nucleic Acids Res.* (2012). doi:10.1093/nar/gkr1029
- 936 70. Cock, P. J. A. *et al.* Biopython: Freely available Python tools for computational molecular  
937 biology and bioinformatics. *Bioinformatics* (2009). doi:10.1093/bioinformatics/btp163
- 938 71. Sugimoto, N. *et al.* Thermodynamic parameters to predict stability of RNA/DNA hybrid  
939 duplexes. *Biochemistry* **34**, 11211–6 (1995).
- 940 72. Mi, H. *et al.* Protocol Update for large-scale genome and gene function analysis with the  
941 PANTHER classification system (v.14.0). *Nat. Protoc.* **14**, 703–721 (2019).
- 942 73. Schymkowitz, J. *et al.* The FoldX web server: an online force field. *Nucleic Acids Res.* **33**,  
943 W382–W388 (2005).
- 944
- 945

946 FIGURE LEGENDS  
947



948 **Figure 1 A simple parsimonious model predicts the most probable outcomes of Target-AID**  
949 **mutagenesis. A)** gRNAs included in the time course base editing experiment had diverse C content pro-  
950 files in the Target-AID activity window. Nucleotides are color coded: guanines are purple, thymine is  
951 red, adenines are green and cytosines are blue. **B)** Overall fraction of edited reads for all target sites rate  
952 along timepoints in the experiment: T0 (start of induction), T6 (mid induction), T12 (end of induction). The  
953 solid time point represents surviving cells plated after galactose induction, while the liquid time point  
954 represents the cell population after canavanine co-selection. Amplification of the *ERO1* target site from  
955 the liquid recovery time points was unsuccessful (shown in grey), and as such the solid recovery time  
956 point was used instead for the other analysis steps. **C)** Fraction of genotypes with different numbers of  
957 edited nucleotides in the Target-AID activity window after co-selection for each locus. Values represents  
958 the fraction of reads with either one, two or three edits compared to the total fraction of reads that were  
959 edited. **D)** Editing outcome type for all sites with a total editing rate greater than one percent after co-  
960 selection (n=30 cytosines across all targeted sites). The C to G/T distribution represents the sum of edit-  
961 ing that resulted in a C to G or C to T mutation. Position-wise editing rates and outcome are shown in  
962 Supplementary Figures 5 and 6. **E)** Agreement between the predicted nucleotide total editing rank in the  
963 model used to predict mutagenesis outcomes in the large-scale experiment and the deep sequencing  
964 data (n=28 sites, 10 gRNAs: gRNA specific predicted and observed rankings are presented in Supple-  
965 mentary Figure 5 and 6). The gRNAs targeting *ADE1* and *SES1* were respectively excluded from the  
966 analysis because there is only one editable site in the activity window and total editing rate was too low.  
967 **F)** Edited read coverage of the mutation outcome prediction model and the 99th percentile of edited allele  
968 combinations (n=4 genotypes in both cases) for the gRNAs with editing activity included in the large-scale  
969 experiment.  
970

971 **Figure 2 A gRNA library for systematic perturbation of essential genes using the Target-AID base**  
972 **editor.** Essential genes (ex.: *E.G. 1*) were scanned for sites appropriate for Target-AID mutagenesis.  
973 Mutational outcomes include silent (grey triangle), missense (black triangle) mutations, as well as stop  
974 codons (\*). DNA fragments corresponding to the gRNA sequences were synthesized as an  
975 oligonucleotide pool and cloned into a co-selection base editing vector. Using gRNAs as molecular  
976 barcodes, the abundance of cell subpopulations bearing mutations is then measured after mutagenesis  
977 and bulk competition. Mutations with fitness effects are inferred from reductions in the relative gRNA  
978 abundances.  
979

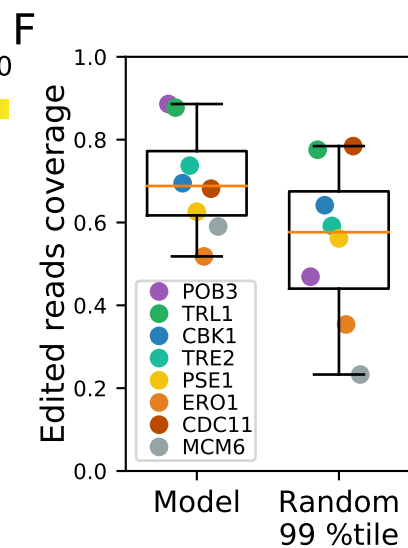
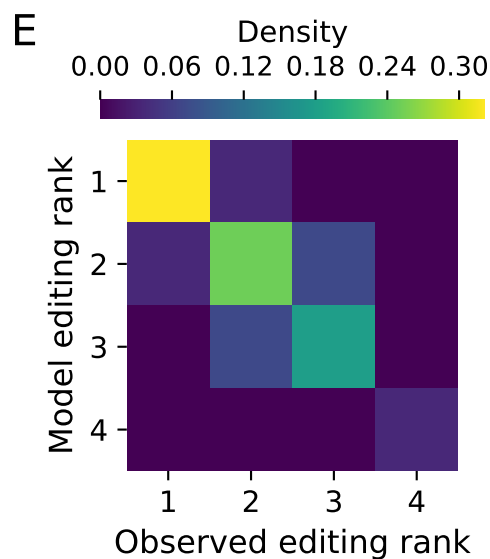
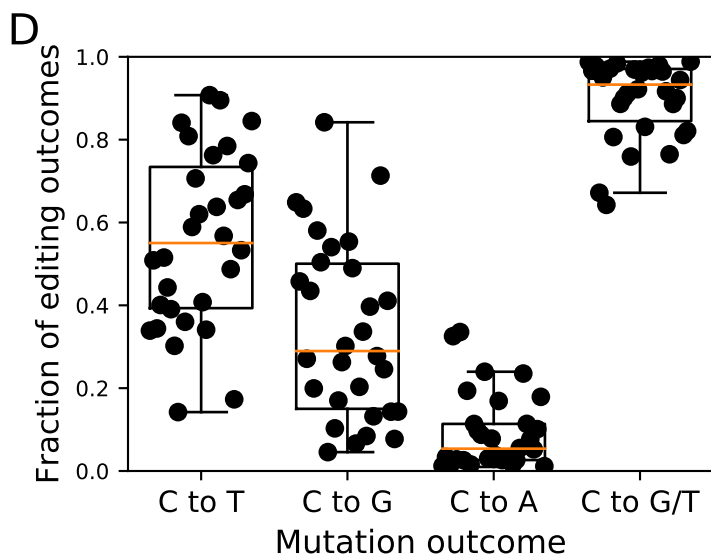
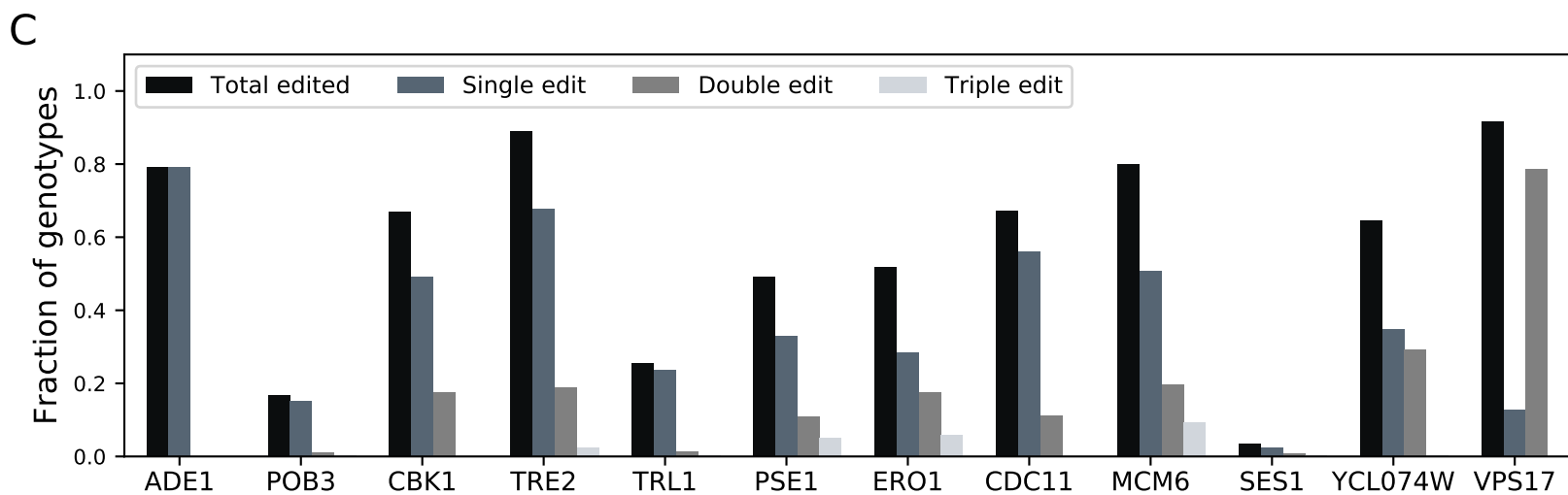
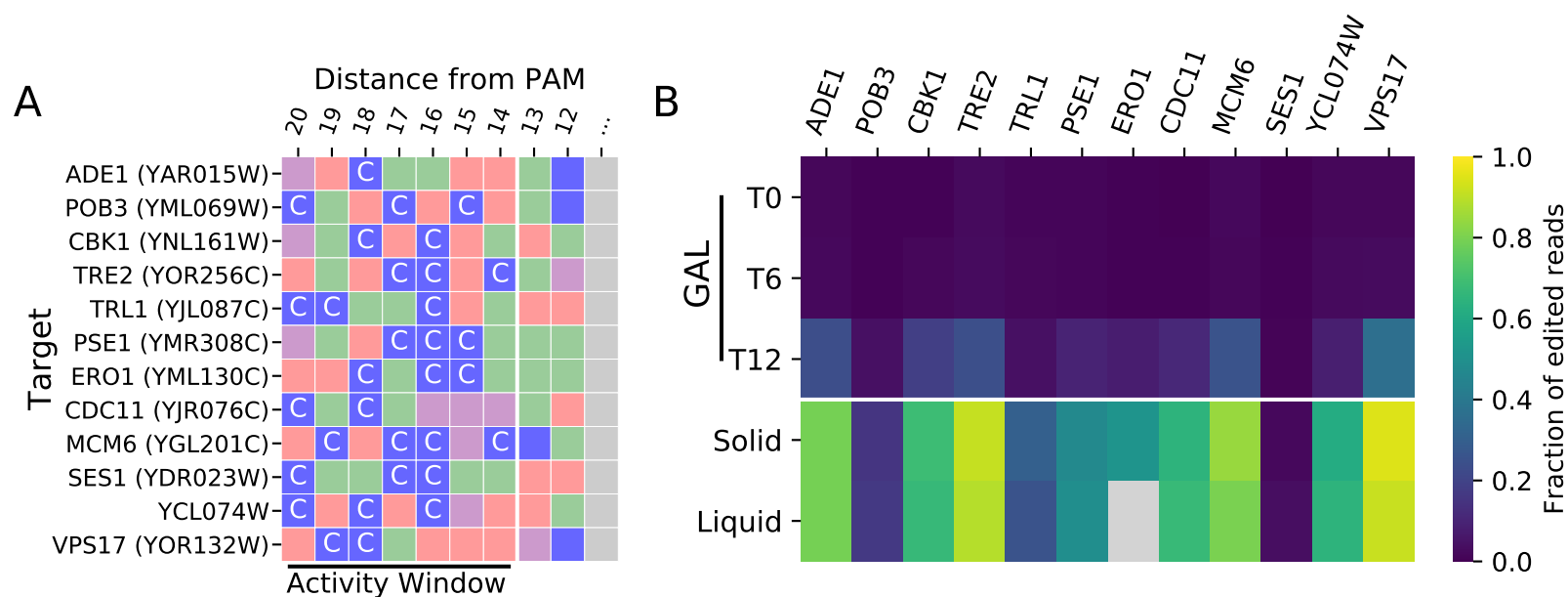
980 **Figure 3. High-throughput forward mutagenesis by Target-AID base editing identifies sensitive**  
981 **sites across the yeast genome. A)** Cumulative distribution of z-scores of the log<sub>2</sub> fold-change in gRNA  
982 abundance between mutagenesis and the end of the bulk competition experiment. Scores were  
983 calculated using the distribution of abundance variation between the start of the experiment and the end  
984 of mock editor induction, the fitted normal distribution is shown as a black line. The z-score threshold was  
985 set at ~5% FDR and is represented by a dotted black line. The distribution of target types in the 1,118  
986 gRNAs with Negative Effects (GNE) is shown in the inset. **B)** Positions of base editing target sites in the  
987 yeast genome. Telomeric regions are depleted in target sites because very few essential genes are  
988 located there. GNEs are shown in red, and other gRNAs are in black. The orientation of the line matches  
989 the targeted strand relative to the annotated coding sequence. **C)** Decline in gRNA abundance (on a log  
990 scale) between timepoints after mutagenesis for gRNAs targeting GLN4, a tRNA synthetase. Median  
991 gRNA abundance across the entire library through time is shown in green. The red lines represent the  
992 gRNAs categorized as having a significant effect (GNE) for this gene, while non-significant gRNAs (NSG)  
993 are shown in black. The gRNA with the most extreme z-score targets residue G267. **D)** Mutagenesis of  
994 GLN4-G267 confirms its essential role for protein function. Tetrad dissection of a heterozygous deletion  
995 mutant bearing an empty vector results in only two viable spores, while the wild-type copy in the same  
996 vector restores growth. Dissection of the two heterozygous mutants bearing a plasmid with the most  
997 probable single mutant based on the known activity window of Target-AID shows both mutations are  
998 lethal.  
999

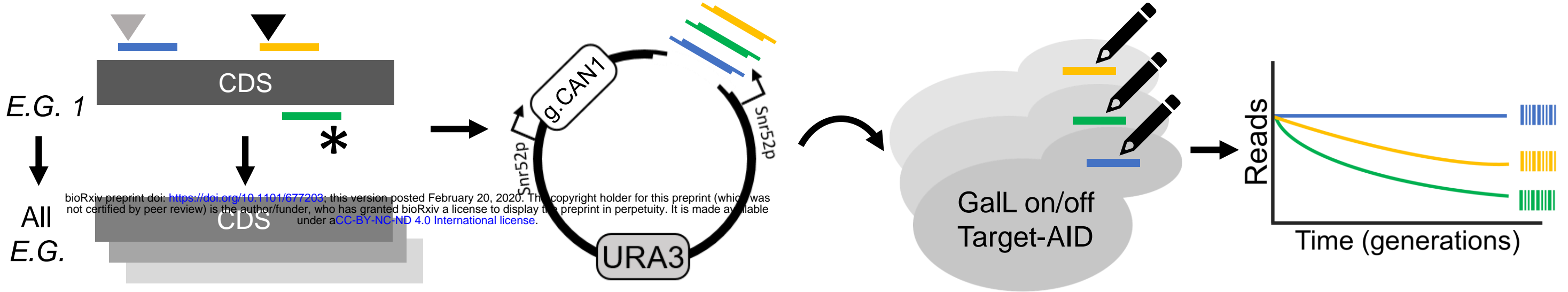
1000 **Figure 4: GNE induced mutations are enriched in predicted deleterious effects A)** SIFT score  
1001 distributions for the most likely induced mutations of both GNEs (blue) and NSGs (red). The thresholds for  
1002 the categories used in the enrichment calculations in **B)** are shown as black dotted lines. SIFT scores  
1003 represent the probability of a specific mutation being tolerated based on evolutionary information: the first  
1004 threshold of 0.05 was set by the authors in the original manuscript<sup>32</sup> but might be permissive considering  
1005 the number of mutations tested in our experiment (n= 895, 12394, 704, 8520, 643, 7396, 508, 5682). All  
1006 GNE vs NSG score comparisons are significant (Welch's t-test p-values:  $1.19 \times 10^{-24}$ ,  $3.01 \times 10^{-24}$ ,  $9.00 \times 10^{-12}$ ,  
1007  $1.55 \times 10^{-12}$ ). The box cutoff is due to the large fraction of mutations for which the SIFT score is 0. B)  
1008 Enrichment folds of GNEs over NSGs for different variant effect prediction measurements. Envision score  
1009 (Env.), SIFT score (SIFT), protein folding stability based on solved protein structures (Struct.  $\Delta\Delta G$ ),  
1010 protein folding based on homology models (Model  $\Delta\Delta G$ ) and protein-protein interaction interface stability  
1011 based on structure data (Inter.  $\Delta\Delta G$ ). The raw values used to calculate ratios are shown in  
1012 Supplementary table 1. The predictions based on conservation and experimental data are grouped under  
1013 'Predictors' and those based on the computational analysis of protein structures and complexes under  
1014 'Structural'.  
1015

1016 **Figure 5 GNE mutations are enriched for specific amino acid substitution patterns and identify**  
1017 **critical sites for protein function. A)** Fold depletion and enrichment volcano plots for the most probable  
1018 mutations induced by GNEs in the screen. Enrichment and depletion values were calculated by  
1019 comparing the relative abundance of each mutation among GNEs and NSGs using Fisher's exact tests.  
1020 Mutation patterns significantly depleted are shown in blue, while those that are enriched are in red. The  
1021 significance threshold was set using the Holm-Bonferroni method at 5% FDR and is shown as a dotted  
1022 grey line. **B)** Protein variant frequency among 1000 yeast isolates (black dots) and residue evolutionary  
1023 rate across species (blue line) for *RAP1*. The target site for the GNEs targeting T486 is highlighted by a  
1024 red line while the other detected GNEs target sites are shown by a grey line. **C)** Tetrad dissections  
1025 confirm most *RAP1* GNE induced mutations indeed have strong fitness effects, as well as other  
1026 substitutions targeting these sites.

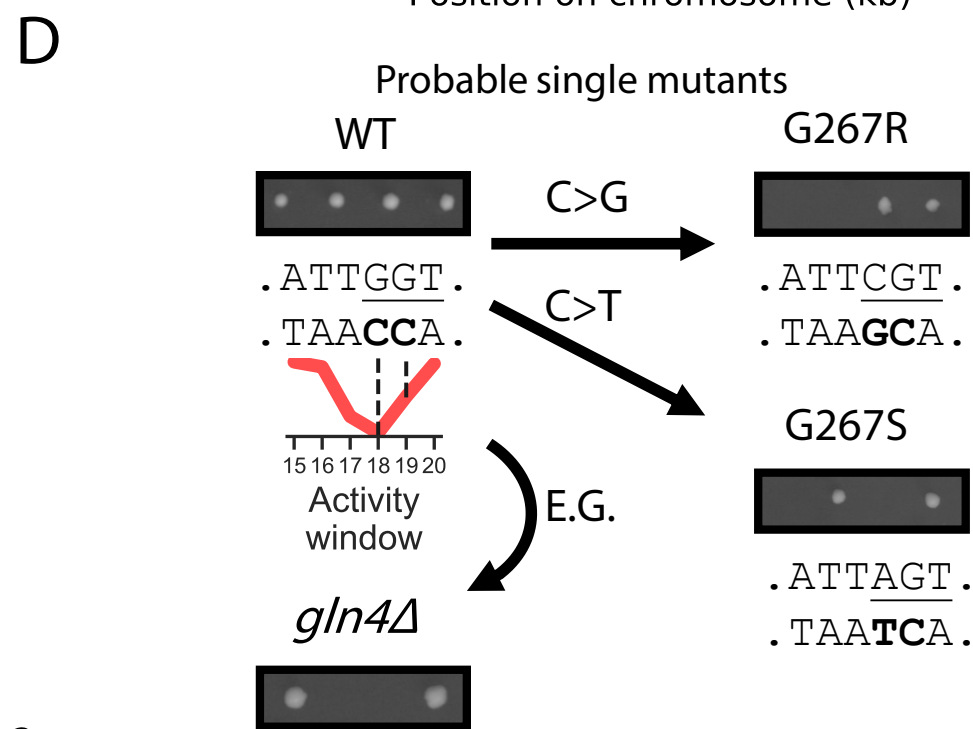
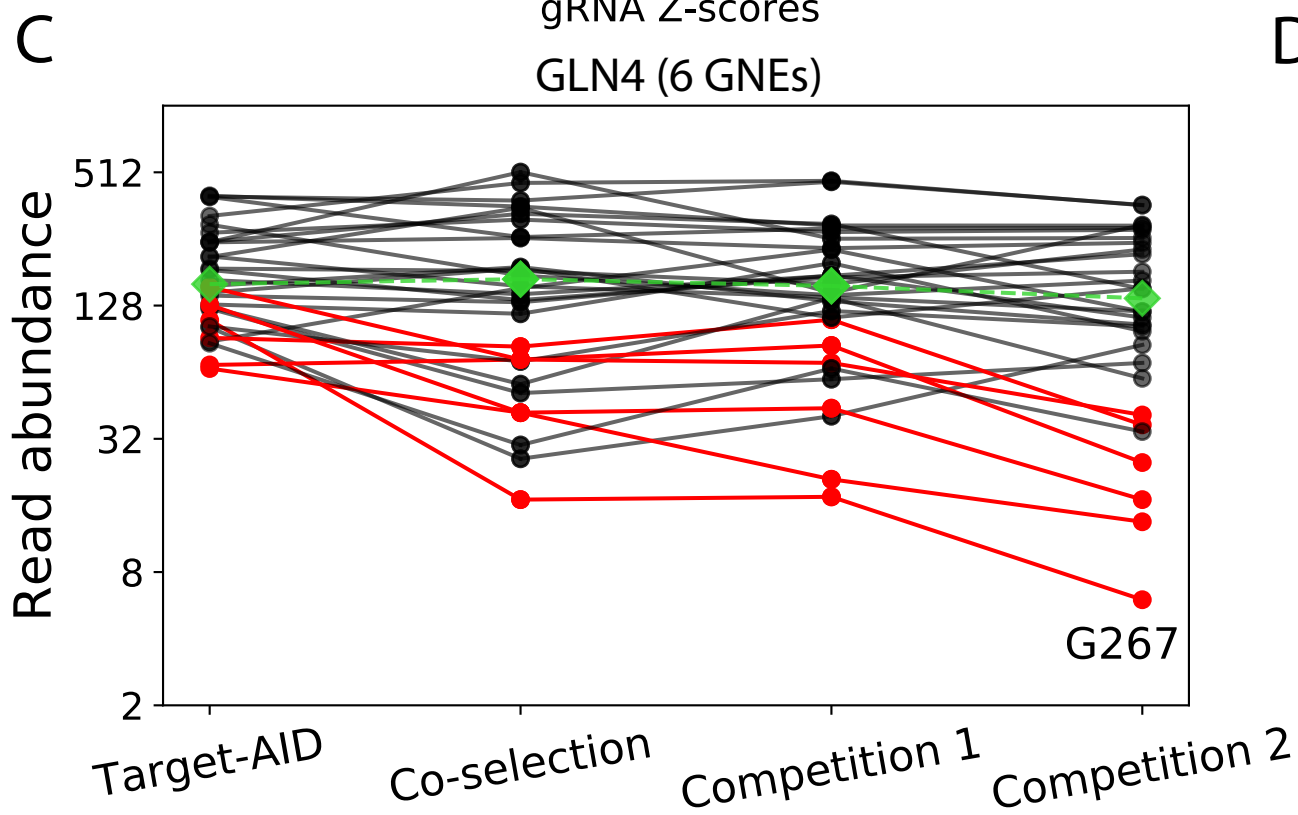
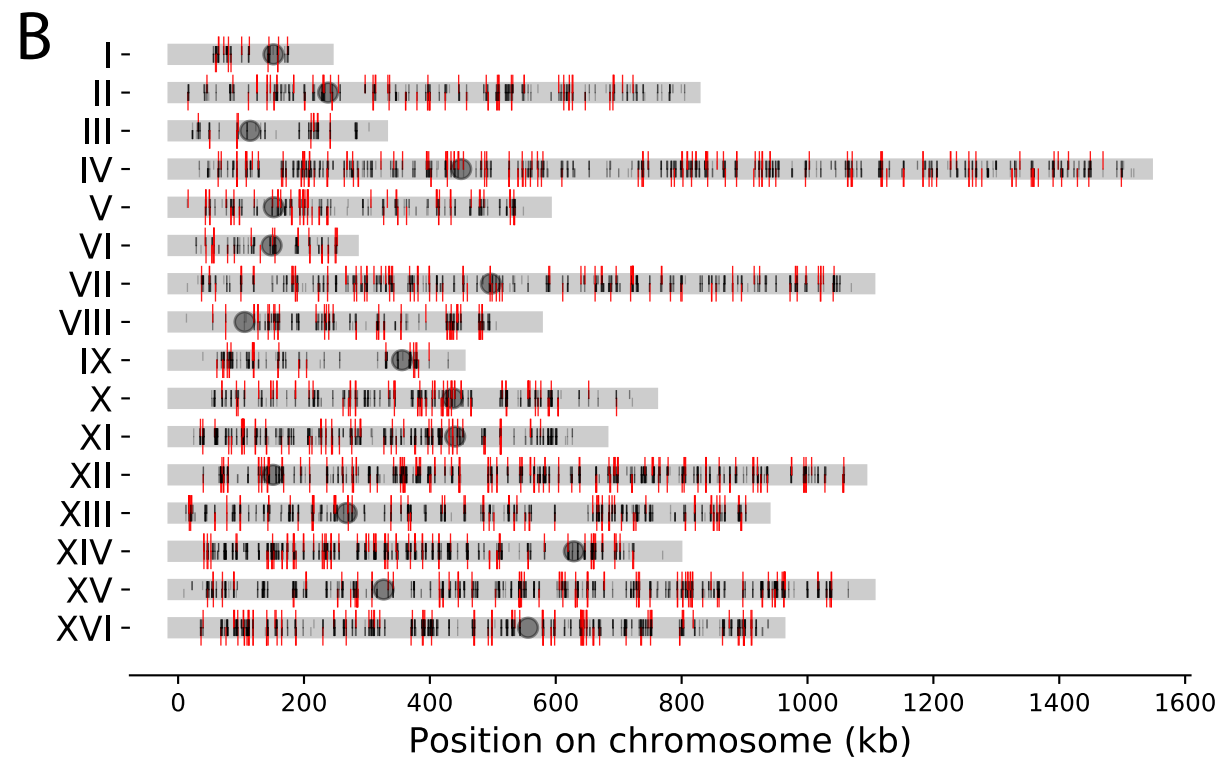
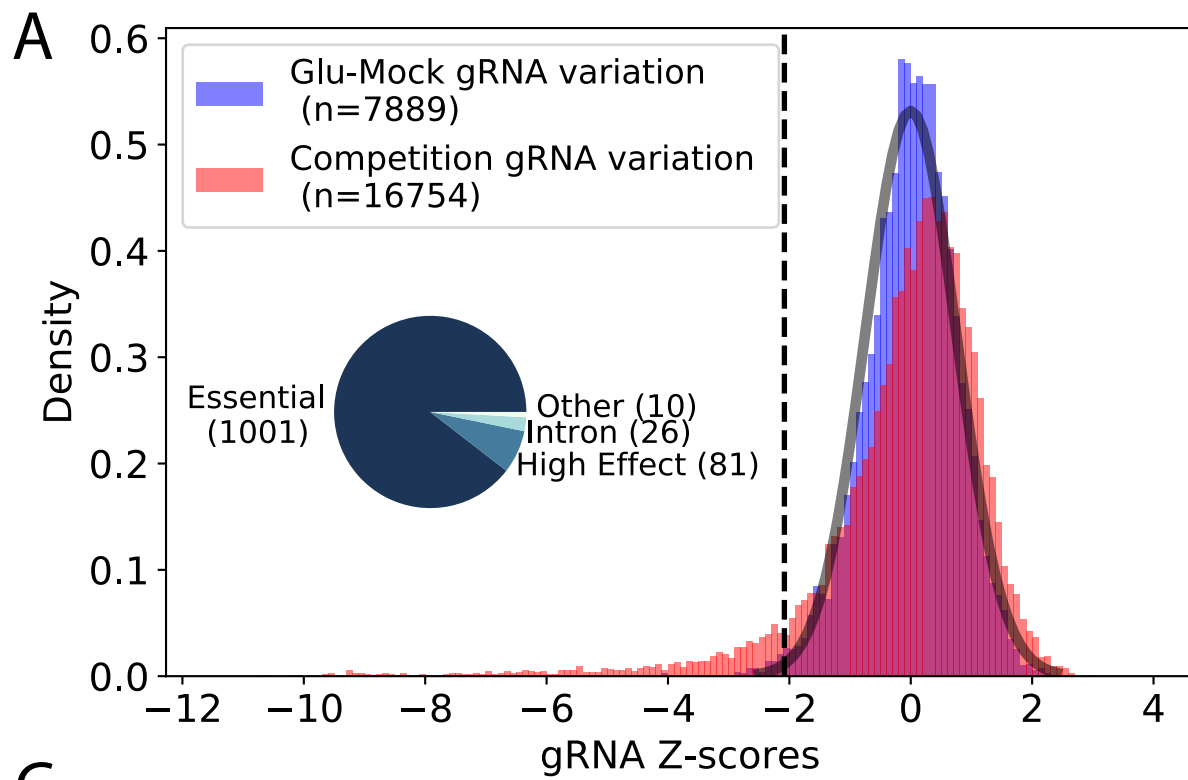
1027

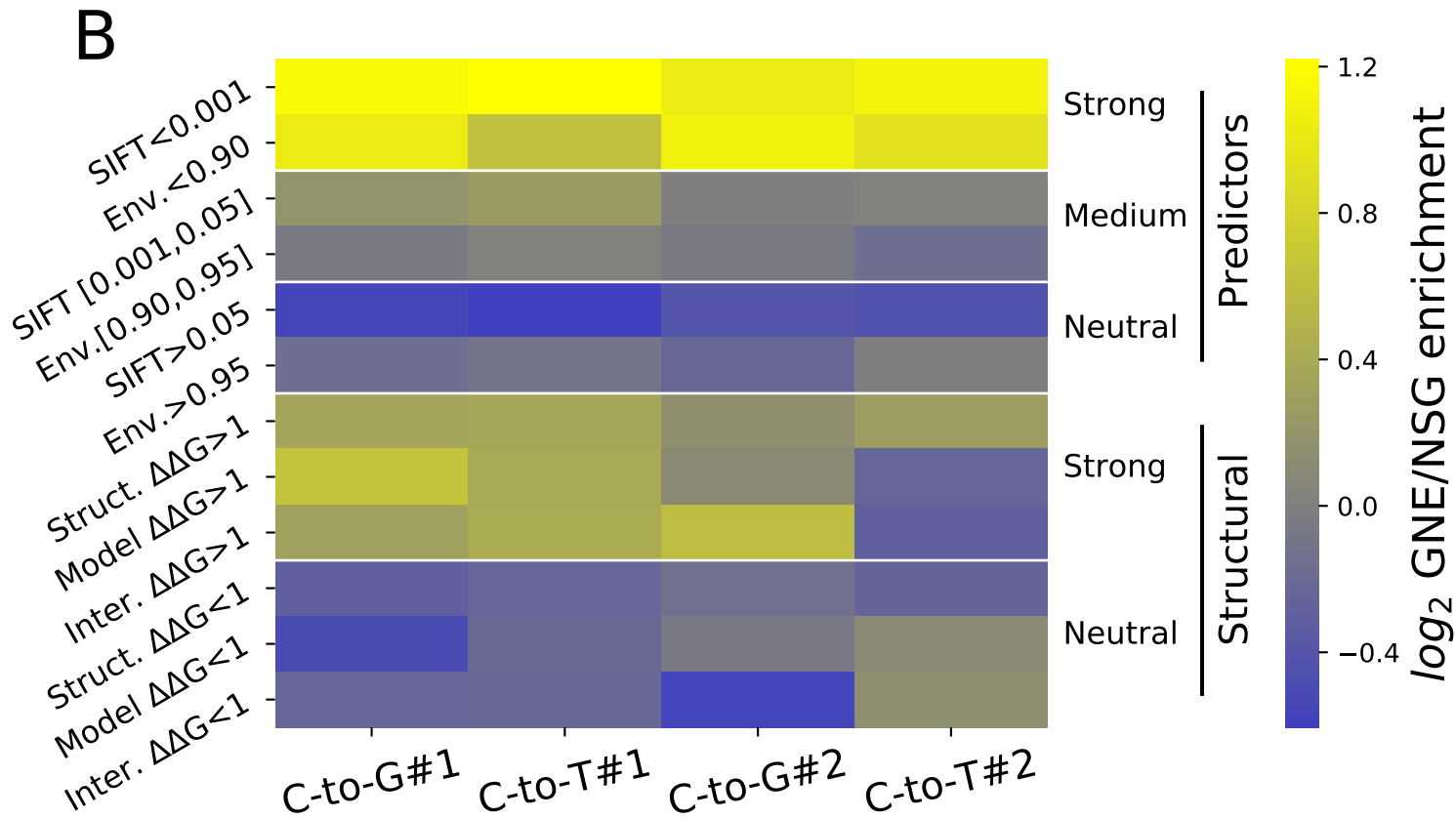
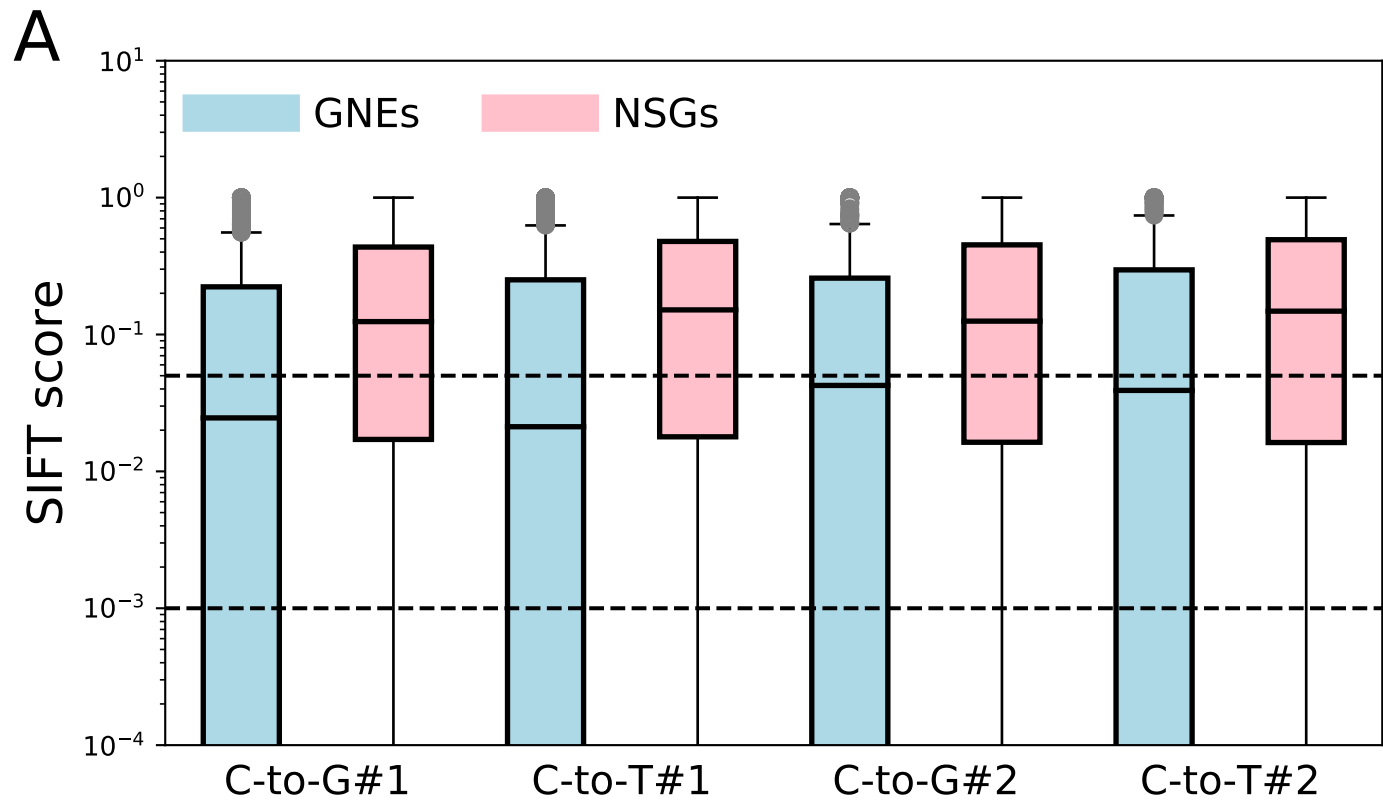
1028 **Figure 6 gRNA and target properties affect mutagenesis efficiency. A)** Since Target-AID can gener-  
1029 ate both C to G and C to T mutations, many codons can be targeted to create premature stop codons.  
1030 The TGG (W) codon is the only one targeted on the non-coding strand as ACC. **B)** GNE ratio for SGGs  
1031 targeting different codons in essential genes, split by co-editing risk categories, were 1 and 2 represent  
1032 low or very low co-editing risk while 3 or 4 represent moderate to high co-editing risk. **C)** Cumulative z-  
1033 score density of SGGs grouped by the mutational outcome generating the stop codon. A higher rate of  
1034 GNE is observed for gRNAs for which a C-to-G mutation at the highest editing activity position generates  
1035 a stop codon mutation. The significance threshold is shown as a black dotted line. **D)** Cumulative z-score  
1036 density of gRNAs that do not generate stop codons targeting either the coding or non-coding strand. **E)**  
1037 SGG and non-SGG GNE enrichment compared to the expected GNE ratio for different melting tempera-  
1038 ture ranges. **F)** gRNA/DNA duplex melting temperature as a function of gRNA GC content for all gRNAs  
1039 for which fitness effects were measured. The higher and lower efficiency thresholds are based on the en-  
1040 richments shown in panel E.  
1041

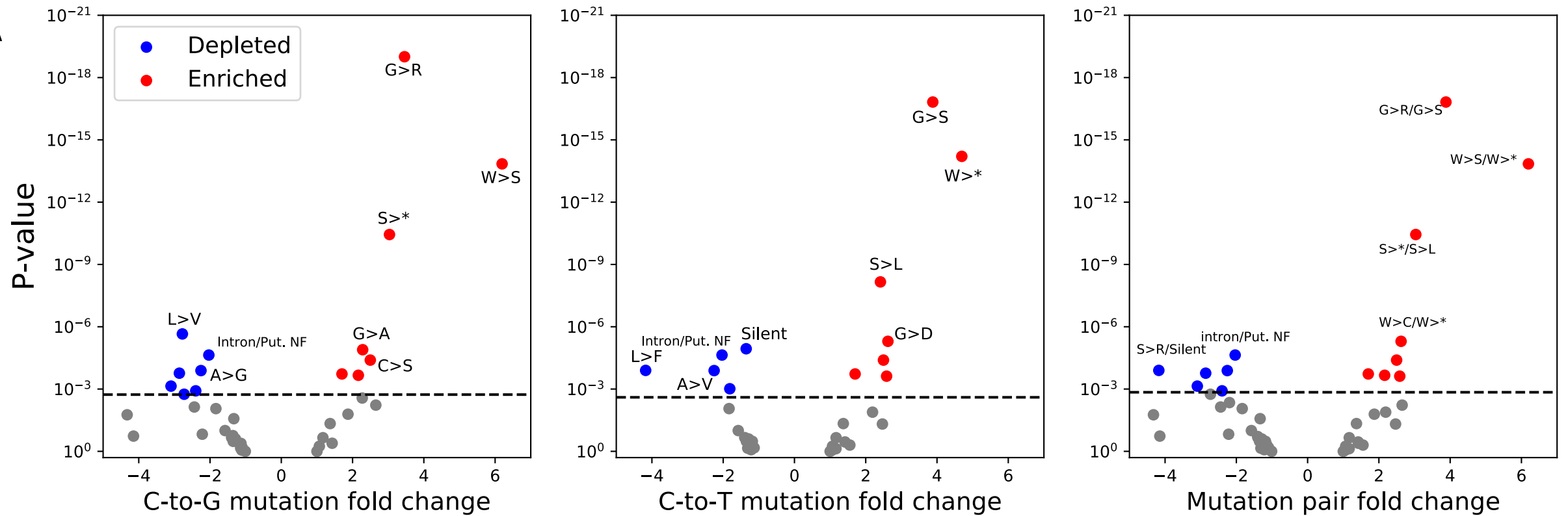
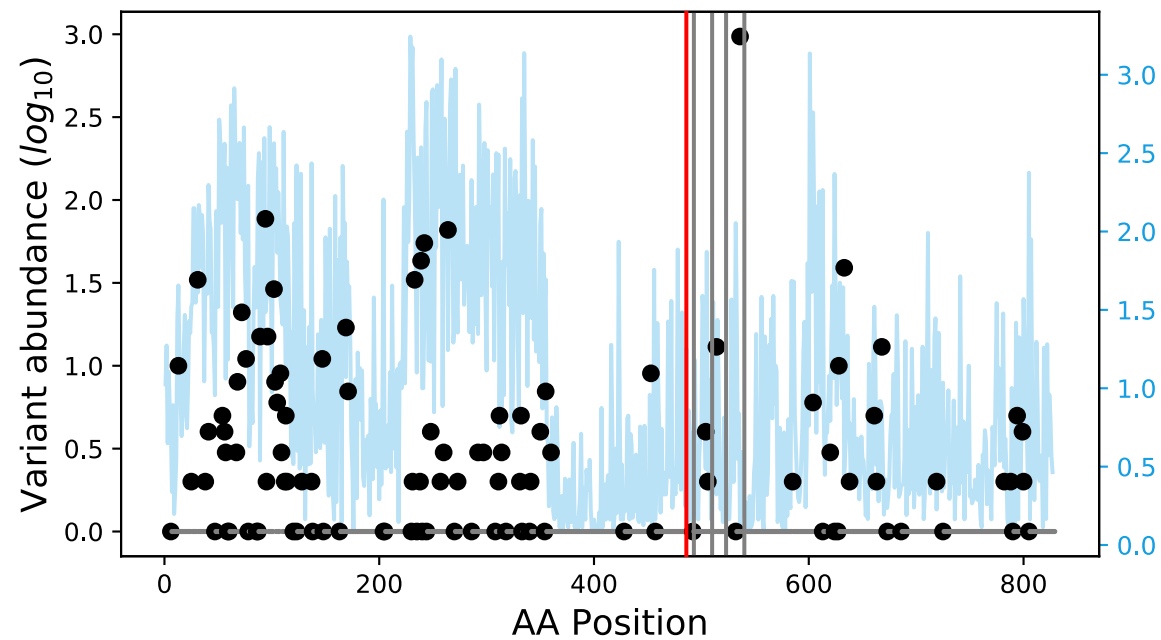










**A****B****C**